minerals

MDPI

Article

PGE-Cu-Ni Mineralization of Mafic-Ultramafic Massifs of the Khangai Upland, Western Mongolia

Maria Shapovalova [1,2,*], Nadezhda Tolstykh [1,2], Roman Shelepaev [1,2] and Valery Kalugin [1]

[1] Sobolev Institute of Geology and Mineralogy of Siberian Branch of Russian Academy of Sciences, Koptyuga Ave., 3, 630090 Novosibirsk, Russia; tolst@igm.nsc.ru (N.T.); rshel@igm.nsc.ru (R.S.); kalugin@igm.nsc.ru (V.K.)

[2] Laboratory of Evolution of Paleo-Oceans and Mantle Magmatism, Department of Geology and Geophysics, Novosibirsk State University, Pirogova St., 1, 630090 Novosibirsk, Russia

* Correspondence: shapovalovam@igm.nsc.ru; Tel.: +7-923-187-9620

Received: 8 September 2020; Accepted: 21 October 2020; Published: 23 October 2020

Abstract: The mafic-ultramafic massifs with the PGE-Cu-Ni mineralization located in North-Central Mongolia: Oortsog, Dulaan, Mankhan, Yamat, and Nomgon were investigated. For the first time we consider these massifs as a single magmatic association and as fragments of Khangai batholith caused by the action of the plume responsible for the formation Permian Khangai LIP. The massifs fractionated from peridotite to gabbro have a similar typomorphic ore mineralogical and geochemical features, which change depending on the degrees of fractionation of magma and evolution of the sulfide melt. The least fractionated Oortsog massif originated from Ni-rich high-Mg basaltic magma. It is characterized by predominance of pyrrhotite mineralization due to exsolution of monosulfide solid solution (MSS). The most fractionated is the Nomgon massif originated from Cu-rich basaltic magma with bornite-chalcopyrite mineralization, formed as an exsolution of intermediate solid solution (ISS). The rest of the massifs have a medium characteristics between these two. The compositions of sulfides in the studied massifs change in accordance with the increase in sulfur fugacity from peridotite to gabbro: enrichment of pentlandite in Ni and pyrrhotite in S. The composition of PGM changes from Pt minerals in Oortsog massif to Pd minerals in Nomgon massif in the same direction. These massifs can be considered as potential for the PGE.

Keywords: Khangai upland; mineralogy; geochemistry; sulfide; PGE-Cu-Ni; PGMs; LIP

1. Introduction

The most economic Cu-Ni-PGE deposits relate to the occurrence of mafic-ultramafic magmatism of large igneous provinces (LIP) [1–3]. Such examples include the unique Cu-Ni-PGE deposits of the Norilsk region, confined to the traps of the Siberian Craton (250 Ma) due to the action of the central part of a deep mantle plume [3]. Cu-Ni-PGE deposits in the south of the Siberian Craton are also associated with mafic-ultramafic magmatism: Fe-Ti-V-Cu-PGE Chiney deposit (1880 Ma), Cu-Ni-PGE Yoko-Dovyren intrusion (728 Ma), and Cu-Ni-PGE Kingash deposit (1410–873 Ma) [4–7]. In addition, PGE-rich Cu-Ni deposits are confined to the central parts of the plumes, such as the Emeishan and Tarim plumes [8–10].

We studied the Permian mafic-ultramafic massifs of the Khangai upland (Oortsog, Dulaan, Mankhan, Yamat, and Nomgon) (Figure 1), which are the early phases of the Khangai batholith [11–13] according to one of the theories of Khangai LIP [14]. The massifs are considered to be the result of the melting of a deep plume and, as a consequence, derivatives of mantle magmatism [15–17]. Therefore, the massifs have ore (PGE-Cu-Ni) potential, which has been confirmed by previous research [18]. Minerals of the platinum group elements or PGE (PGMs: sperrylite, isoferroplatinum, etc.) were

found in schlich samples of the Oortsog and Nomgon massifs, which are an indicator of the potential platinum-bearing of mafic-ultramafic intrusions [19]. Revealing metallogeny of mafic-ultramafic intrusions of Khangai LIP is great scientific and predictive value.

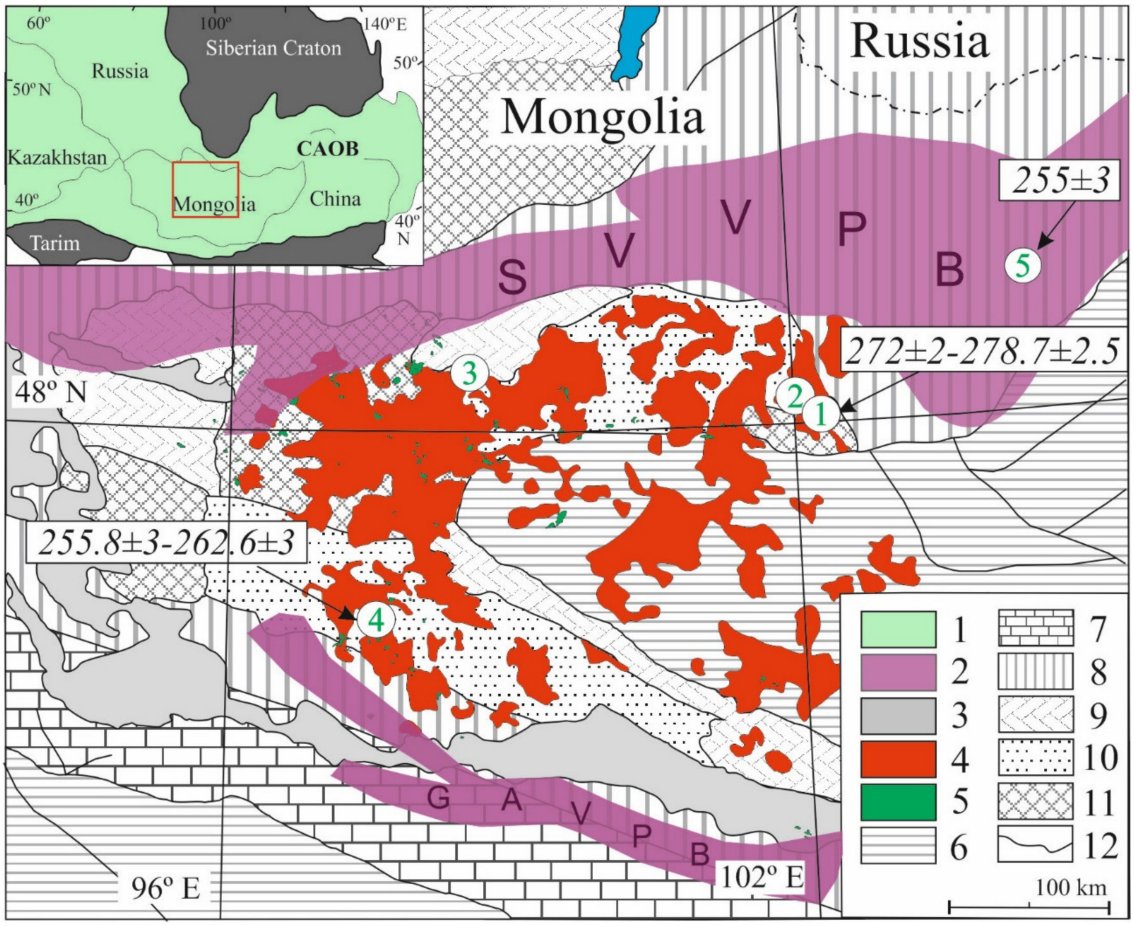

Figure 1. A geologic map of the mafic-ultramafic massifs in Khangai batholith (after [20]). 1—Central Asian Orogenic Belt (CAOB); 2—volcano-plutonic belt; 3—Mesozoic–Cainozoic troughs; 4—Late Paleozoic granitoids of the Khangai batholith; 5—Permian gabbros of the Khangai uplands; 6–9—orogens: 6—Middle-Late Paleozoic (Hercynides), 7—Early-Middle Paleozoic (late caledonides), 8—Vendian-Early Paleozoic (early Caledonides), 9—Neoproterozoic; 10—tectonic blocks with the Early Precambrian basement; 11—tectonic blocks with the Pre-Vendian orogenic basement; 12—main tectonic boundaries. Figures in circles show studied mafic-ultramafic massifs of Permian age: 1—Oortsog; 2—Dulaan; 3—Mankhan; 4—Yamat; 5—Nomgon. SVVPB—Selenga–Vitim volcano-plutonic belt, GAVPB—Gobi–Altay volcano-plutonic belt.

This article presents the mineralogy-geochemical features of the PGE-Cu-Ni sulfide mineralization found in different host rocks from the massifs of the Khangai upland, where samples of the Mankhan and Yamat massifs was collected for the first time. This allowed comparing them with other massifs (Oortsog, Dulaan, and Nomgon) [18,21–23], to supplement the data on their evolution and to reveal the patterns of formation of sulfide mineralization in that region of the Central Asian Orogenic Belt (CAOB). In the end, we propose ore forming processes, evolution of sulfide melt, and composition of parent magma.

2. Geological Setting

The sulfide-bearing massifs of the Khangai upland are located in North-Central Mongolia in the south-eastern area of the CAOB (Figure 1). The CAOB is the largest Phanerozoic juvenile orogenic

belt in the world and evolved over some 800 Ma. It is located between the East European, Siberian, North China, and Tarim cratons and encompasses an immense area of Russian from the Urals, through Altai-Sayan and Transbaikalia to the Okhotsk Sea, and areas of Kazakhstan, Kyrgyzstan, Uzbekistan, Mongolia, Northwestern China, and Northeast China [24]. The CAOB is composed of fragments of Precambrian continental blocks and Paleozoic island arcs, ophiolites, and volcanic rock assemblages, which were formed during action of various geodynamic processes [25–29].

The Khangai upland is represented by the Khangai batholith bounded by the Selenga-Vitim volcano-plutonic belt to the north and the Gobi-Altay volcano-plutonic belt to the south [30]. A group of giant (>0.2 km^3) batholiths formed in the CAOB in the Late Paleozoic and Early Mesozoic: Angara-Vitim (305–280 Ma), Khangai (269–241 Ma), and Khentei (230–195 Ma) distributed over Western Transbaikalia, Northern Mongolia, and NE China, respectively [31–34]. The Khangai batholith consists of an association of synplutonic rocks: granitoids and rocks of basic-intermediate composition, among which small intrusions have been identified [11]. These include the studied massifs: Oortsog, Dulaan, Mankhan, and Yamat. The Nomgon massif is part of Selenga-Vitim volcano-plutonic belt (SVVPB) (Figure 1).

The evolution of the Khangai magmatic region is much debated. Some researchers proposed that the formation of both the batholith and volcano-plutonic belts was in an active continental margin and intraplate (mantle plume) settings, where the Khangai magmatic area is regarded as a LIP [11,35,36]. Another group of scientists suggests that those granitic batholith and volcano-plutonic belts were formed by the subduction of the Mongol-Okhotsk Ocean beneath an active continental margin of the Siberian continent to the north or were emplaced in a back-arc setting [34,37–41].

3. Geology, Petrology, and Age of Massifs

The layered Oortsog peridotite–troctolite–gabbro massif has been studied in more detail than other massifs [42], and is representative of a layered intrusion with PGE-Cu-Ni-mineralization. The massif consists of rhythmically layered peridotite and gabbroid (Intrusion 1), and poorly differentiated biotite-bearing amphibole–olivine gabbro and gabbronorite (Intrusion 2). Typical outcrops of gabbroids, including sulfide-bearing gabbroids, are shown in the Figure 2a,b. The rocks of the earlier Intrusion 1 have lower contents of incompatible elements including alkalis (Table 1, Figure 3) than the later Intrusion 2. The rocks of Intrusions 1 and 2 were derived from depleted (positive εNd) and enriched (negative εNd) mantle sources, respectively [42]. The olivine mezogabbro of Intrusion 1 is 278 ± 2.5 Ma (^{39}Ar-^{40}Ar) and the Bt-bearing olivine mezogabbro of the Intrusion 2 is 272 ± 2 Ma (U-Pb, SHRIMP-II). These data indicate that the Oortsog massif has a Permian age.

The Dulaan massif is located 1.5 km northwest of the Oortsog massif. It consists of strongly altered olivine gabbro with normal alkalinity (Figure 3b). The fractionation trend of the Dulaan massif is similar to the trend of the Oortsog massif on the MgO vs. Al_2O_3 diagram (Figure 3a). According to [18] the Dulaan massif is considered to be promising for Cu-Ni ores.

The Mankhan massif located in the north of the Khangai upland (Figure 1) consists of gabbro and gabbronorite. The MgO content varies within narrow limits (4.00–7.90 wt%), while the rocks have a slightly increased alkalinity (1.23–3.10 wt%) compared to the Oortsog and the Dulaan massifs.

The Yamat massif located in the south of the study region (Figure 1) is a large magmatic body, the scale of which has not been fully established. According to previous studies [43], the massif consists of three intrusions. The late Intrusion 3 is represented by monzogabbro, where the alkali content reaches 6.5 wt%. Monzogabbro is enriched with incompatible elements, such as the Intrusion 2 of the Oortsog massif. The SHRIMP U-Pb zircon dating gives ages of 255.8 ± 2.9 Ma (Intrusion 1) and 262.6 ± 3.1 Ma (Intrusion 2) for olivine mezogabbro and Bt-bearing olivine mezogabbro, respectively [43]. This indicates the Permian age of the massif.

Figure 2. Photos of outcrops. (**a**) Layered gabbro of the Oortsog massif; (**b**) lumps of gabbro with oxidized sulfide droplets; (**c**) sample of Bt-Hbl-bearing mezogabbro with disseminated sulfides; (**d**) the preparation with sulfides droplets mounted in epoxy resin and polished.

The Nomgon massif is located in the northeast of the Khangai upland on the periphery of the Khangai batholith into SVVPB (Figure 1). The massif belongs to the troctolite-anorthosite-leucogabbro formation. The Nomgon massif is rhythmically-layered with a predominance of leucocratic gabbroids and anorthosites; plagioperidotites are found at the base of the rhythms. The rocks of this massif have an olivine-plagioclase fractionation trend, which is moved toward leucocratic compositions (Figure 3a) with alkali contents from 0.65 to 2.39 wt% (Figure 3b). According to previous research [18,21–23,44] the Nomgon massif contains Pt and Pd: 0.3 ppm and 0.6 ppm, respectively.

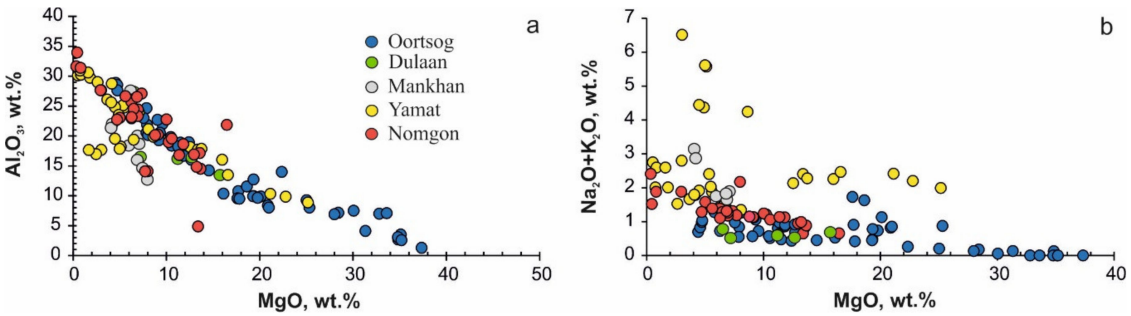

Figure 3. MgO vs. Al_2O_3. (**a**) (Na_2O + K_2O); (**b**) of mafic-ultramafic rocks of the Khangai upland.

Thus, mafic-ultramafic massifs located in the Khangai upland have a single trend of rock fractionation, a similar rare-earth composition of the rocks, and a Perm age of origin [45–47]. Sulfide mineralization was found in all massifs and one represented by disseminated and droplet-like types.

Table 1. Rock compositions (wt%) in mafic-ultramafic massifs of the Khangai upland.

Intrusion	Oortsog					Dulaan		Mankhan		Yamat			
	1		2							1	2		3
SiO_2	45.28	45.47	45.56	45.02	43.85	42.82	38.53	41.18	39.47	44.23	43.81	44.98	51.50
TiO_2	0.18	0.20	0.52	0.38	0.28	0.84	1.97	1.69	1.74	0.53	0.36	0.48	1.18
Al_2O_3	17.43	17.30	9.89	8.40	8.02	16.36	16.55	15.86	14.54	26.83	15.86	24.61	17.77
Fe_2O_3	7.99	7.29	12.12	12.59	14.61	14.67	19.54	19.32	21.78	5.40	12.57	7.11	9.96
MnO	0.11	0.11	0.17	0.17	0.20	0.17	0.15	0.23	0.23	0.08	0.16	0.08	0.15
MgO	12.77	12.61	20.11	20.93	25.27	11.35	7.23	6.81	7.37	2.91	15.83	5.24	4.98
CaO	14.31	14.63	9.78	11.12	6.01	14.14	15.60	12.13	12.54	13.64	7.63	12.68	7.82
Na_2O	0.66	0.65	0.78	0.58	0.56	0.54	0.47	1.51	1.24	2.40	1.67	1.94	3.73
K_2O	0.07	0.10	0.35	0.24	0.32	0.08	0.05	0.13	0.09	0.31	0.56	0.42	1.87
LOI	0.52	0.78	0.69	0.55	0.58	0.04	0.02	0.49	0.60	2.13	1.27	1.88	−0.25
Total	99.75	99.76	100.66	100.74	100.35	101.19	100.33	99.55	99.82	99.11	100.31	99.84	99.32
Rocks	Ol mezogabbro	Ol mezogabbro	Melanogabbro	Mezogabbro	Mezogabbro	Ol mezogabbro	Ol mezogabbro	Leucogabbro	Mezogabbro	Mezogabbro	Hbl mezogabbro	Bt-Hbl mezogabbro	Bt-Hbl mezzo-gabbronorite
Sample	MO1-16	MO3-16	B13043	B13052	B13060	Ch41-14	Ch43-14	Sh138-17	Sh143-17	Sh228-14	Sh104-14	Sh220-14/3	Sh235-14

4. Sampling and Analytical Methods

A sample collection (Figure 2c) of ultramafic and mafic rocks was gathered during field works conducted in 2014–2018 on the Khangai upland in Mongolia. The analyses in this study were carried out in the Analytical Center for multi-elemental and isotope research of the Sobolev Institute of Geology and mineralogy SB RAS in Novosibirsk, Russia. The rock compositions were determined by XRF using an ARL 9900 (Thermo Fisher Scientific, Ecublens, Switzerland) (analyst N. Karmanova) (Table 1).

Several samples of rocks with PGE-Cu-Ni mineralization from all massifs were prepared (sorted manually and mounted in epoxy resin, thereafter polished) (Figure 2d). The composition of ore minerals was studied using a scanning-electron microscope Mira 3 (Tescan, Brno, Czech Republic) with an energy dispersive spectrometer (EDS Oxford X-Max 80, Oxford Instruments, High Wycombe, UK) (analyst A. Titov). X-ray microanalysis of ore minerals (420 analyses) was carried out using a JXA-8100 (Jeol, Tokyo, Japan) by a method described previously [48]. Calibration was conducted according to the internal standards of minerals and alloys. Analysis was at an accelerating voltage of 20 kV, a probe current of 40 nA, and an accumulation time of 10 s (analyst O. Khmel'nikova). An AXIO LAB.A1 POL microscope (Carl Zeiss Microscopy GmbH, Germany) was used to study polished sections of ores in reflected light.

PGM grains were selected from sulfide-bearing samples of the Oortsog massif (B13060) and Nomgon massif (B13106) (approximately 0.5–0.7 kg each) after crushing and gravitational concentration in water and heavy liquids (bromoform $CHBr_3$). The chemical compositions of the PGMs and texture of the mineral aggregates and separate grains were examined by a LEO-1450VP scanning electron microscope (SEM) (Carl Zeiss AG, Oberkochen, Germany) with the INCA Energy 350 microanalysis system (Oxford Instruments Ltd. Oxford, UK) equipped with EDS, operating at an accelerating voltage of 20 kV, current intensity of 0.4 nA, 50 s measuring time, and beam diameter of ~1 μm (analyst M. Khlestov). Microprobe WDS analyses of PGMs were carried out at 20 kV and 20–30 nA, on a Camebax-micro microprobe (beam size ~1 mm) (analyst O. Khmel'nikova). The following X-ray lines were selected: Lα for Pt, Pd, Rh, Ag, Ir, Ru, Te, Sn, and As; Kα for S, Fe, Cu, Ni, and Co; Mα for Au, Bi, Os, and Pb. The accuracy and reproducibility of the analytical procedures were evaluated with special tests [49].

The contents of the ore elements (Ni, Cu, Co, Zn, Cr, S) were determined by Atomic Absorption Spectrophotometers Analyst 800 (Perkin-Elmer, Waltham, MA, USA) with electrothermal atomizer TGGA and flame atomizer at the Vinogradov Institute of Geochemistry SB RAS in Irkutsk, Russia (analysts G. Pogudina, T. Voronova, and O. Proydakova). The contents of PGE (Os, Ir, Ru, Rh, Pt, Pd, and Au) were determined by an Element 2 Finnigan MAT Inductively Coupled Plasma Mass Spectrometer (ICP-MS) at the same Institute (V. Vlasova, Yu. Sokol'nikova). The total procedural blank was 0.00022 μg/L for Os; 0.0017 μg/L for Ir; 0.0024 μg/L for Ru; 0.019 μg/L for Pt; 0.026 for Pd; and 0.0016 μg/L for Rh.

5. Results

5.1. Sulfide Mineralization

All of the studied massifs host the sulfide mineralization represented by two assemblages: chalcopyrite-pentlandite-pyrrhotine (Oortsog, Dulaan, Yamat) and cubanite-bornite-chalcopyrite (Nomgon) (Figure 4). The Mankhan massif is characterized by an intermediate assemblage (pyrrhotine-chalcopyrite). The Dulaan and Mankhan massifs contain the rare disseminated sulfides (Figure 5a,d) while the sulfides of the Oortsog, Yamat, and Nomgon massifs are represented by disseminated and schlieren types (droplets, globules) (Figure 5b,e,f).

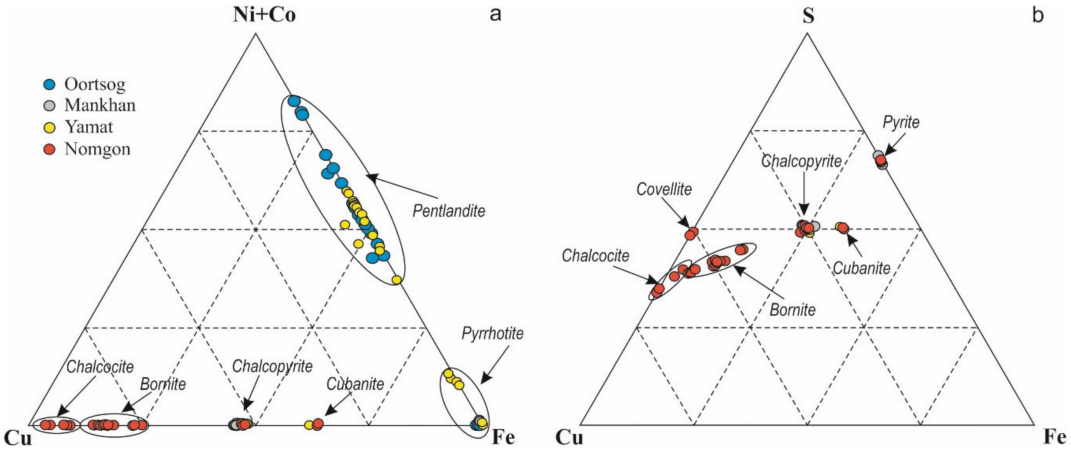

Figure 4. Variety of sulfides in mafic-ultramafic massifs of the Khangai upland: (**a**) Cu-Fe-Ni+Co; (**b**) Cu-Fe-S.

Chalcopyrite-pentlandite-pyrrhotite assemblage of the Oortsog massif has been described previously [50]. Co-pentlandite is present in the Oortsog massif. The proportion of pentlandite and chalcopyrite increases with the increase of the leucocratic ratio of the rocks, therefore, these minerals are much more common in the late intrusions of the massifs. There is a similar sulfide mineralization in the Yamat massif. The sulfides of the Dulaan massif were not considered in this work because the massif is exposed to oxidation and secondary alteration to iron hydroxides. Disseminated sulfide in the Oortsog and Yamat massifs comprise intergrowth of pyrrhotite, pentlandite, and chalcopyrite with a predominance of pyrrhotite (~70–80 vol%). Pyrrhotite can occur as interstitial disseminations in a silicate matrix. Cubanite and mackinawite are less abundant.

Pirrhotite. The sulfide assemblage of the biotite (Bt)-bearing mezogabbro of Intrusion 2 in the Oortsog massif consists of hexagonal pyrrhotite with troilite lamellae (Figure 5c). The pyrrhotite compositions are shown in the Fe(+Co,Cu)–S–Ni diagram (Figure 6a). Troilite (FeS) and hexagonal pyrrhotite ($Fe_{1-x}S$) are found in both massifs and their compositions occur as continuous solid solution FeS-$Fe_{1-x}S$). Troilite contains Ni (up to 0.49 wt%), as the hexagonal pyrrhotite (up to 0.14 wt%). The content of Co in the pyrrhotite reaches up to 0.33 and 0.16 wt% in the rocks of Oortsog and Ymat massifs, respectively. The change of compositions from troilite to hexagonal pyrrhotite is due to the evolution of rock composition from plagioperidotite to leucogabbro [50]. Thus, the proportion of sulfur in pyrrhotite increases with an increase of the leucocratic rock ratio in the series that indicates an increase of sulfur activity during the development of magmatic and ore-forming systems in the Oortsog massif.

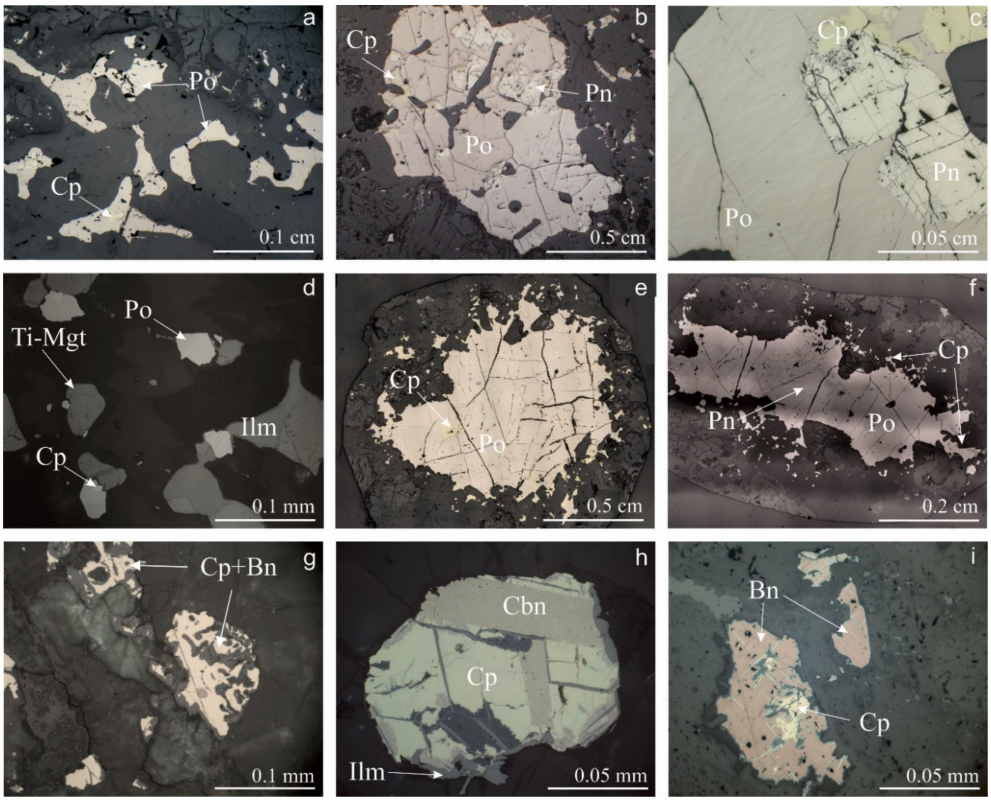

Figure 5. Microphotographs in reflected light of sulfides mineralization in the mafic-ultramafic massifs of the Khangai upland. (**a**–**c**) Ortsog massif: (**a**) interstitial sulfides; (**b**) sulfide droplet of chalcopyrite-pentlandite-pyrrhotite composition; (**c**) fine lamelaes of troilite in hexagonal pyrrhotite; (**d**) disseminated sulfides in rocks of the Mankhan massif; (**e**,**f**) large droplets of sulfides in the Yamat massif; (**g**–**i**) disseminated sulfides in the Nomgon massif of cubanite-bornite-chalcopyrite composites. Po—pyrrhotite, Pn—pentlandite, Cp—chalcopyrite, Bn—bornite, Cbn—cubanite, Ti-Mgt—titanomagnetite, Ilm—ilmenite.

Pentlandite $(Fe,Ni)_9S_8$ occurs as two structural and morphological types in both the Oortsog and Yamat massifs. Pentlandite I is represented by coarse-grained clusters of granular grains (less often), which are usually in intergrowth with pyrrhotite, and rarely with chalcopyrite. Pentlandite II is found as lamellaes within pyrrhotite grains in the rocks of late intrusions of massifs. The Co contents of the pentlandite vary from 3.38 (Pn I) to 15.28 wt% (Pn II) in the Oortsog massif, and from 2.10 (Pn I) to 14.49 wt% (Pn II) in the Yamat massif. Some of the analyses refer to cobaltpentlandite [51], in which the Co content exceeds the sum (Ni + Fe), reaching to 45 wt%. The Fe content predominates over Ni in all pentlandite grains (Table 2). Compositions of pentlandite show the Fe–Ni solid solution in the Fe(+Co,Cu)–S–Ni diagram, where the Fe/Ni ratio varies from 1.41 to 0.92 (Figure 6b). The Ni/(Ni + Fe) ratio in pentlandite grains varies in the range of 0.41–0.52 in Oortsog, and 0.38–0.51 in Yamat massifs, and increases with the increase of the ratio of leucocratic rocks. T. The Co/Ni ratio in pentlandites increases in the same direction: from 0.12 to 0.66 in the Oortsog massif and from 0.27 to 0.61 in the Yamat massif.

Chalcopyrite ($CuFeS_2$) is found in all intrusions as intergrowth with other sulfides, mainly in the interstices of pyrrhotite grains. The composition chalcopyrite is close to stoichiometry (Table 2). Electron-microprobe analyses (WDS) show that Co and Ni contents are detected in small amounts (up to 0.11 wt%).

Table 2. Composition of sulfides (wt%) in mafic-ultramafic massifs of the Khangai upland shown in Figure 4.

№	Mineral	Fe	Co	S	Ni	Cu	Total	Formula
					Oortsog			
1	Po	61.04	0.07	38.66	0.21	-	99.98	$(Fe_{8.99}Ni_{0.04})_{9.03}S_{9.97}$
2		61.20	0.16	38.65	-	-	100.07	$(Fe_{9.02}Co_{0.02})_{9.04}S_{9.96}$
3		62.71	0.07	36.66	-	-	99.49	$Fe_{0.99}S_{1.01}$
4		63.09	0.08	35.99	-	-	99.16	$Fe_{1.00}S_{1.00}$
5		60.87	0.09	38.99	0.23	-	100.18	$(Fe_{8.94}Ni_{0.03}Co_{0.01})_{8.98}S_{10.02}$
6		61.11	0.08	38.98	0.24	-	100.41	$(Fe_{8.96}Ni_{0.03}Co_{0.01})_{9.00}S_{10.00}$
7		60.63	0.13	38.65	0.33	-	99.74	$(Fe_{8.95}Ni_{0.05}Co_{0.01})_{9.01}S_{9.99}$
8		63.36	0.07	35.89	-	-	99.33	$Fe_{1.00}S_{1.00}$
9	Pn	31.05	7.23	33.05	29.48	-	100.82	$(Fe_{4.27}Ni_{3.84}Co_{0.94})_{9.05}S_{7.95}$
10		30.01	8.76	32.90	28.63	-	100.31	$(Fe_{4.14}Ni_{3.75}Co_{1.15})_{9.05}S_{7.95}$
11		29.89	8.08	32.99	29.49	0.11	100.55	$(Fe_{4.12}Ni_{3.86}Co_{1.06})_{9.05}S_{7.95}$
12		29.15	8.31	33.18	29.89	-	100.56	$(Fe_{4.01}Ni_{3.91}Co_{1.09})_{9.01}S_{7.99}$
13		32.14	4.60	33.28	30.40	-	100.47	$(Fe_{4.42}Ni_{3.97}Co_{0.60})_{8.99}S_{8.01}$
14		25.30	15.28	32.97	25.47	-	99.06	$(Fe_{3.53}Ni_{3.38}Co_{2.03})_{8.94}S_{8.06}$
15		31.59	4.77	32.85	29.58	-	98.80	$(Fe_{4.41}Ni_{3.92}Co_{0.63})_{8.97}S_{8.03}$
16		37.19	3.38	32.66	25.03	-	98.28	$(Fe_{5.21}Ni_{3.33}Co_{0.45})_{8.99}S_{8.01}$
17	Co-pn	11.84	45.99	32.73	10.01	-	100.58	$(Co_{6.07}Fe_{1.65}Ni_{1.32})_{9.04}S_{7.96}$
18		13.53	42.15	32.82	11.29	-	99.79	$(Co_{5.59}Fe_{1.89}Ni_{1.50})_{8.98}S_{8.02}$
19	Cp	30.36	0.11	34.40	0.09	34.09	99.04	$Cu_{0.99}Fe_{1.01}S_{2.00}$
20		29.78	0.06	34.24	-	34.47	98.56	$Cu_{1.01}Fe_{0.99}S_{2.00}$
21		30.45	0.03	34.59	-	34.07	99.14	$Cu_{0.99}Fe_{1.01}S_{2.00}$
					Mankhan			
22	Po	59.72	0.32	39.09	0.05	-	99.19	$(Fe_{6.97}Co_{0.04})_{7.01}S_{7.99}$
23		60.04	0.08	38.85	0.33	-	99.31	$(Fe_{7.01}Ni_{0.04})_{7.05}S_{7.95}$
24		60.48	0.08	38.63	0.27	-	99.47	$(Fe_{8.95}Ni_{0.04})_{8.99}S_{10.01}$
25		60.74	0.08	38.55	0.13	-	99.51	$(Fe_{8.99}Ni_{0.02}Co_{0.01})_{9.02}S_{9.98}$
26		60.67	0.10	38.48	0.18	-	99.42	$(Fe_{8.99}Ni_{0.03})_{9.02}S_{9.98}$
27	Cp	30.47	0.04	34.67	-	33.86	99.05	$Cu_{0.98}Fe_{1.01}S_{2.01}$
28		29.87	0.03	34.63	-	33.94	98.47	$Cu_{0.99}Fe_{0.99}S_{2.02}$
29		30.21	0.03	34.60	-	34.68	99.52	$Cu_{1.00}Fe_{1.00}S_{2.00}$
30	Py	46.00	0.03	53.13	-	-	99.16	$Fe_{0.99}S_{2.01}$
31		47.22	0.06	53.79	-	-	101.07	$Fe_{1.00}S_{2.00}$
32		47.37	0.07	53.40	-	-	100.87	$Fe_{1.01}S_{1.99}$

Table 2. *Cont.*

Yamat								
33	Po	61.23	-	38.43	0.20	-	99.88	$(Fe_{9.04}Ni_{0.03})_{9.07}S_{9.93}$
34		63.11	0.05	37.50	0.14	0.22	101.04	$Fe_{0.98}S_{1.02}$
35		63.10	-	36.55	-	-	99.72	$Fe_{0.99}S_{1.01}$
36		62.85	-	35.84	-	-	98.75	$Fe_{1.00}S_{1.00}$
37		63.80	-	36.33	-	-	100.17	$Fe_{1.00}S_{1.00}$
38		63.23	-	35.81	-	-	99.07	$Fe_{1.00}S_{1.00}$
39	Pn	27.14	11.13	32.75	27.79	-	98.81	$(Fe_{3.80}Ni_{3.69}Co_{1.48})_{8.97}S_{8.03}$
40		28.16	14.49	33.12	23.91	0.07	99.77	$(Fe_{3.90}Ni_{3.15}Co_{1.91})_{8.96}S_{8.04}$
41		30.28	12.21	33.01	24.32	-	99.88	$(Fe_{4.19}Ni_{3.20}Co_{1.60}Cu_{0.01})_{9.00}S_{8.00}$
42		30.74	9.95	32.92	26.15	0.26	100.05	$(Fe_{4.25}Ni_{3.43}Co_{1.31}Cu_{0.03})_{9.03}S_{7.97}$
42		31.36	10.25	33.18	25.84	-	100.66	$(Fe_{4.31}Ni_{3.37}Co_{1.34})_{9.02}S_{7.98}$
43		55.86	2.10	36.21	4.88	-	99.05	$(Fe_{7.95}Ni_{0.63}Co_{0.27})_{8.85}S_{8.15}$
44	Cp	30.95	0.08	34.79	0.09	34.19	100.10	$Cu_{0.98}Fe_{1.02}S_{2.00}$
45		30.59	-	34.52	-	34.23	99.35	$Cu_{0.99}Fe_{1.01}S_{2.00}$
46		30.86	-	34.70	0.06	34.29	99.95	$Cu_{0.99}Fe_{1.01}S_{2.01}$
47	Cbn	40.63	-	35.16	-	23.32	99.11	$Cu_{1.00}Fe_{1.99}S_{3.01}$
48		39.53	-	35.11	-	24.32	98.95	$Cu_{1.04}Fe_{1.94}S_{3.02}$
Nomgon								
49	Cp	30.63	-	34.60	-	34.76	100.00	$Cu_{1.00}Fe_{1.01}S_{1.99}$
50		30.39	-	34.76	-	34.90	100.05	$Cu_{1.00}Fe_{1.00}S_{2.00}$
51		30.16	-	34.40	-	33.95	98.52	$Cu_{0.99}Fe_{1.00}S_{2.01}$
52	Cbn	40.62	-	35.11	-	23.28	99.02	$Cu_{1.00}Fe_{1.99}S_{3.01}$
53		40.70	-	34.80	-	23.38	98.88	$Cu_{1.01}Fe_{2.00}S_{2.99}$
54	Bn	10.97	-	25.82	-	63.18	100.02	$Cu_{4.97}Fe_{0.98}S_{4.05}$
55		10.50	-	25.15	-	63.05	98.70	$Cu_{5.03}Fe_{0.96}S_{4.01}$
56		10.91	-	25.30	-	62.58	98.80	$Cu_{4.98}Fe_{0.99}S_{4.03}$
57	Cv	-	-	30.62	-	65.16	95.78	$Cu_{1.03}S_{0.97}$
58	Cc	-	-	20.57	-	77.41	97.98	$Cu_{1.96}S_{1.04}$
59		-	-	20.40	-	79.47	99.87	$Cu_{1.98}S_{1.02}$
60	Py	46.19	-	53.01	-	-	99.20	$Fe_{1.00}S_{2.00}$
61		46.30	-	53.02	-	-	99.32	$Fe_{1.00}S_{2.01}$

Note. Sulfides (1–4, 9–12) from Intrusion 1 of Oortsog massif, (5–8, 13–16)—Intrusion 2 of Oortsog massif. Nomenclature of sulfides [52]: Po—pyrrhotite, Pn—pentlandite, Cp—chalcopyrite, Cbn—cubanite, Bn—bornite, Cv—covellite, Cc—chalcocite, Py—pyrite. "–"—below detection limit.

Bornite-cubanite-chalcopyrite assemblage was described earlier in the Nomgon massif [18,21] where chalcopyrite predominates. Chalcopyrite includes minor amount of Co and Ni (Table 2). Cubanite is present in trace amounts as exsolution lamellae in chalcopyrite, because it is an exsolution product of a high-temperature intermediate solid solution (ISS) [53]. Chalcopyrite is usually replaced by bornite with the formation of rims or complete pseudomorphs (Figure 5i). Chalcocite and covellite are found as replacement products of chalcopyrite and bornite.

The disseminated mineralization of the Nomgon massif is a rare type of copper deposits associated with layered ultramafic-mafic intrusions [54]. A similar association resulting from the evolution of ISS was recently described in the Talnakh massive ores [55]. Sulfides in the Nomgon massif occur in the intergranular space of silicates, and do not include rock-forming minerals (olivine, plagioclase), therefore, sulfides are formed after crystallization of silicate minerals. The chalcopyrite predominates over other sulfides in the Mankhan massif (Figure 5d). Hexagonal pyrrhotite occurs as intergrowth with chalcopyrite and contains Co and Ni (0.08–0.32 wt% and 0.13–0.33 wt%, respectively). Pyrite was found in the Mankhan and Nomgon massifs as cubic crystals in the intergranular space of silicates. Compositions of pyrites are given in Table 2.

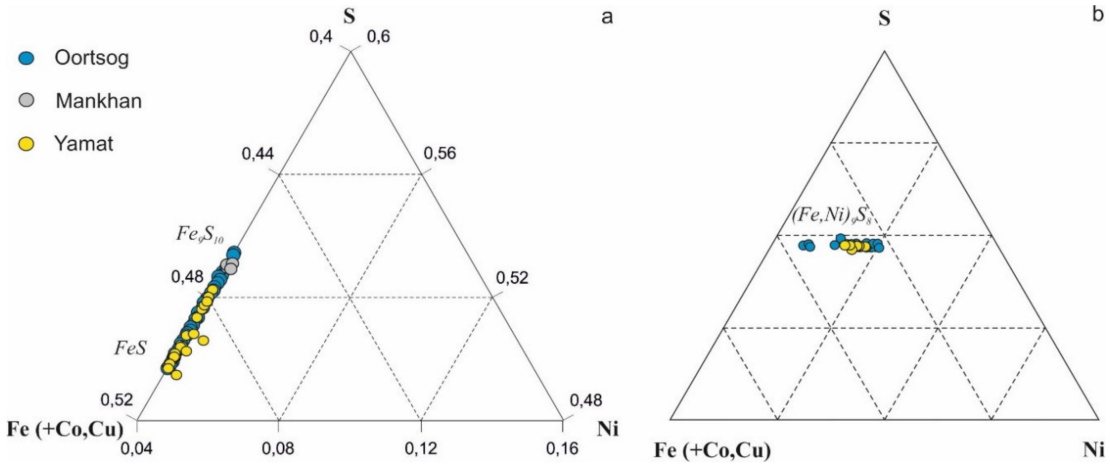

Figure 6. The composition of sulfides in the mafic-ultramafic massifs of the Khangai upland on the Fe(+Co,Cu)–S–Ni diagram: (**a**) pyrrhotite; (**b**) pentlandite.

5.2. Noble Metal Mineralization

We investigated PGMs (Figure 7) from heavy concentrate of crushing samples and schlich samples from the Oortsog and Nomgon massifs. The PGE mineralization in the Nomgon massif was previously studied [22,23], in which it was found that the Rh-bearing sperrylite is more common. In addition, merthieite-II, isomertieite, stibiopalladinite, majakite, kotulskite, keithconnite, merenskyite, melonite, and michenerite were found. We repeated the findings of these PGMs, adding to the list of minerals with froodite $Pd(Bi,Te)_2$, Au-Ag alloys, and hollingworthite (RhAsS)–sperrylite ($PtAs_2$) solid solution (Figure 7g–i). PGMs were also found in rocks of the Oortsog massif [50,56] in a heavy concentrate of sample B-13060 as rare grains (20–50 μm): sperrylite in intergrowth with cobaltite, pyrrhotite, and maucherite (Figure 7a), and braggite (Pt,Pd,Ni)S (Figure 7b). Some PGMs are spatially associated with base-metal sulfides. Au-Ag alloys were also found in this assemblage. In addition, euhedral crystals of sperrylite and isoferroplatinum were found in a schlich sample of the Oortsog massif (Figure 7d-f) [50]. These minerals are indicative in placer aureoles; their discovery indicates that the massifs are promising in relation to PGE [18,19].

Compositions of sperrylite from bedrock from the Oortsog massif contain Fe, Co, and Ni (tenths of a percent), whereas sperrylite from schlich samples of the Nomgon massif is Rh-rich (up to 4.35 wt%) (Table 3). The solid solutions of hollingworthite–sperrylite grains contain Os (up to 2.39 wt%). The Au/Ag ratios

in Au-Ag alloys of both massifs are close to 1:1. These alloys in the Oortsog massif contain Cu (2.72 wt% on average) and Fe (0.71 wt% on average), while in the Nomgon they are free of minor elements.

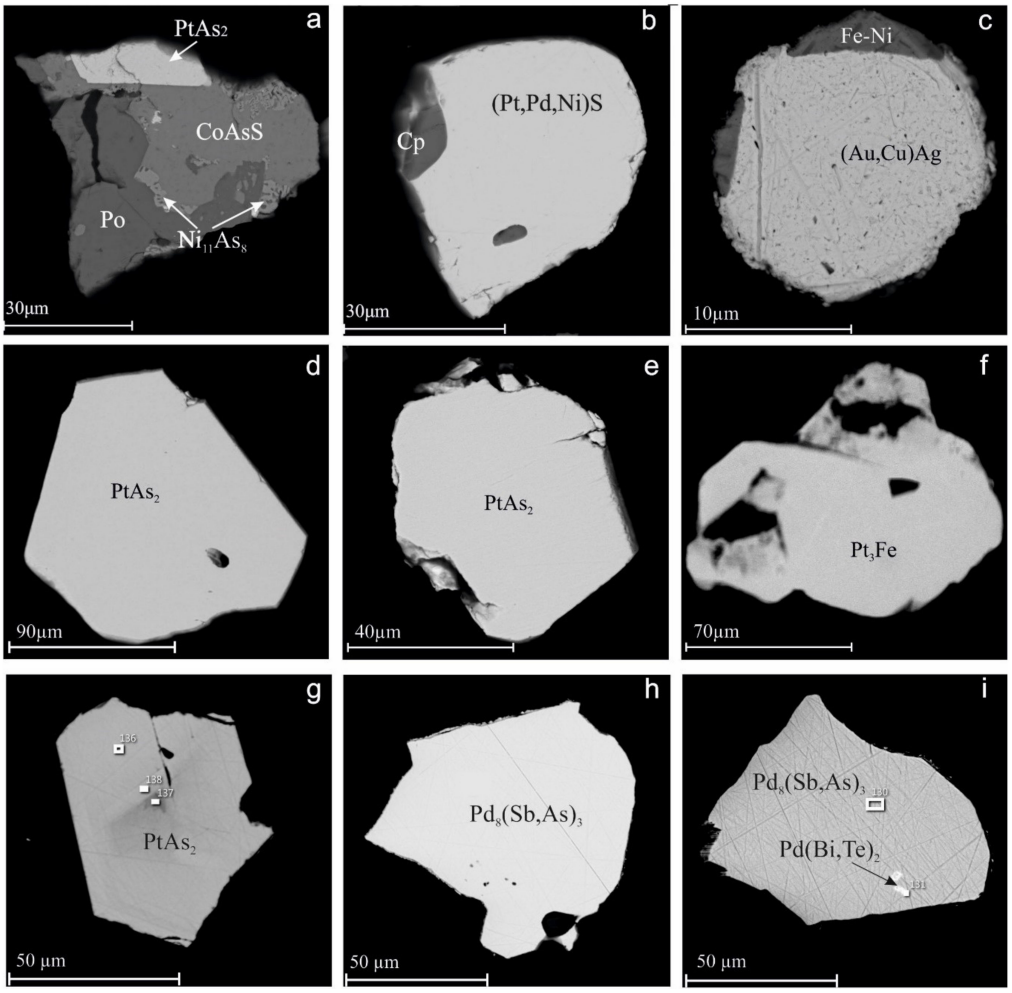

Figure 7. Minerals of precious metals from a heavy concentrate of crushing samples from the Oortsog (**a**–**c**) and Nomgon (**g**–**i**) massifs, and from the schlich samples of the Oortsog massif (**d**–**f**): (**a**) intergrowths of sperrylite with cobaltite (CoAsS), pyrrhotite (Po) and maucherite ($Ni_{11}As_8$), (**b**) braggite Pt(S,Pd,Ni) with chalcopyrite (Cp), (**c**) Au-Ag alloy, (**d**,**e**,**g**) sperrylite crystals ($PtAs_2$), (**f**) isoferroplatinum crystal (Pt_3Fe), (**h**) grain of mertieite-II, (**i**) froodite inclusion $Pd(Bi,Te)_2$ in mertieite-II. Rectangles in images (**g**–**i**) areas of SEM analysis.

5.3. Geochemistry of Ore Elements

The rocks of different composition from all intrusions of the massifs of the Khangai upland were analyzed for the ore elements (Ni, Cu, Co, Cr, and S), PGE (Os, Ir, Ru, Rh, Pt, and Pd), and Au (Table 4).

Table 3. Composition of PGE minerals and Au-Ag alloys (wt%) in mafic-ultramafic massifs of the Khangai upland.

№	Mineral	Fe	Co	Ni	Cu	Au	Ag	Pt	Pd	Os	Rh	Sb	As	S	Total	Formula
Oortsog																
1	Sperrylite	0.61	0.32	0.40	-	-	-	56.68	-	-	-	-	41.12	0.23	99.37	$(Pt_{1.00}Fe_{0.04}Ni_{0.02}Co_{0.02})_{1.08}(As_{1.89}S_{0.03})_{1.92}$
2		0.90	0.50	0.41	-	-	-	53.9	-	-	-	-	39.03	0.24	94.97	$(Pt_{1.00}Fe_{0.05}Ni_{0.03}Co_{0.02})_{1.10}(As_{1.87}S_{0.03})_{1.90}$
3		-	-	-	-	-	-	56.02	-	-	-	-	42.88	-	98.90	$Pt_{1.10}As_{1.90}$
4		-	-	-	-	-	-	57.13	-	-	-	-	42.66	-	99.79	$Pt_{1.09}As_{1.91}$
5		-	-	-	-	-	-	56.91	-	-	-	-	42.08	-	98.99	$Pt_{1.11}As_{1.89}$
6	Braggite	-	-	1.41	-	-	-	75.44	9.64	-	-	-	-	16.24	102.74	$(Pt_{0.77}Pd_{0.18}Ni_{0.05})_{1.00}S_{1.00}$
7		-	-	1.21	-	-	-	76.98	8.16	-	-	-	-	15.76	102.11	$(Pt_{0.80}Pd_{0.16}Ni_{0.04})_{1.00}S_{1.00}$
8	Electrum	0.48	-	-	2.69	58.61	35.85	-	-	-	-	-	-	-	97.63	$Ag_{0.49}Au_{0.44}Cu_{0.06}Fe_{0.01}$
9		0.96	-	0.82	2.75	58.76	36.9	-	-	-	-	-	-	-	100.18	$Ag_{0.48}Au_{0.42}Cu_{0.06}Fe_{0.02}Ni_{0.02}$
Nomgon																
10	Sperrylite	-	-	-	-	-	-	50.21	-	-	4.08	-	42.55	1.92	98.77	$(Pt_{0.78}Rh_{0.18})_{0.96}(As_{1.76}S_{0.28})_{2.04}$
11		-	-	-	-	-	-	51.04	-	-	4.35	-	43.5	2.09	101.91	$(Pt_{0.83}Rh_{0.13})_{0.96}(As_{1.84}S_{0.18})_{2.04}$
12		-	-	-	-	-	-	52.98	-	-	-	-	42.39	1.40	96.77	$(Pt_{0.91}Rh_{0.05})_{0.96}(As_{1.95}S_{0.09})_{2.04}$
13		-	-	-	-	-	-	53.37	-	-	1.88	-	43.72	0.98	99.94	$Pt_{0.93}(As_{1.98}S_{0.09})_{2.07}$
14		-	-	-	-	-	-	54.74	-	-	-	-	42.86	0.82	98.42	$Pt_{0.97}As_{2.03}$
15		-	-	-	-	-	-	55.58	-	-	-	-	43.41	0.59	99.58	$Pt_{0.98}As_{2.02}$
16		-	-	-	-	-	-	55.79	-	-	-	0.89	43.04	-	99.72	$Pt_{0.99}As_{2.01}$
17	Hollingworthite	-	-	-	-	-	-	26.59	-	2.39	24.21	-	37.08	10.36	100.62	$(Rh_{0.59}Pt_{0.34}Os_{0.03})_{0.96}(As_{1.24}S_{0.80})_{2.04}$
18		-	-	-	-	-	-	28.75	-	2.12	22.60	-	36.55	9.39	99.40	$(Rh_{0.57}Pt_{0.38}Os_{0.03})_{0.98}(As_{1.26}S_{0.76})_{2.02}$
19		-	-	-	-	-	-	31.03	-	-	20.15	-	37.51	8.17	97.91	$(Rh_{0.50}Pt_{0.41})_{0.91}(As_{1.28}S_{0.81})_{2.09}$
20	Majakite	-	0.54	23.95	-	-	-	-	43.64	-	-	1.27	31.72	-	101.12	$Pd_{0.99}(Ni_{0.97}Co_{0.02})_{0.99}(As_{1.00}Sb_{0.02})_{1.02}$
21		-	0.40	24.03	-	-	-	-	43.92	-	-	1.16	31.4	-	100.9	$Pd_{0.98}(Ni_{0.98}Co_{0.02})_{1.00}(As_{1.00}Sb_{0.02})_{1.02}$
22		1.35	-	19.82	-	-	-	-	44.12	-	-	2.78	26.16	-	94.51	$Pd_{1.07}(Ni_{0.88}Fe_{0.08})_{0.96}(As_{0.91}Sb_{0.06})_{0.97}$
23	Mertieite -II	-	-	-	0.96	-	-	-	65.69	-	-	25.9	3.03	-	95.59	$(Pd_{7.67}Cu_{0.19})_{7.86}(Sb_{2.64}As_{0.50})_{3.14}$
24		-	-	-	1.35	-	-	-	68.45	-	-	27.76	2.73	-	100.29	$(Pd_{7.62}Cu_{0.25})_{7.87}(Sb_{2.70}As_{0.43})_{3.13}$
25		-	-	-	1.22	-	-	-	68.47	-	-	31.89	-	-	101.58	$(Pd_{7.66}Cu_{0.23})_{7.89}Sb_{3.11}$
26		-	-	-	1.5	-	-	-	68.85	-	-	28.05	2.63	-	101.03	$(Pd_{7.60}Cu_{0.28})_{7.88}(Sb_{2.71}As_{0.41})_{3.12}$
27		-	-	-	1.25	-	-	-	68.96	-	-	27.86	3.15	-	101.22	$(Pd_{7.60}Cu_{0.23})_{7.83}(Sb_{2.68}As_{0.49})_{3.17}$
28		-	-	-	1.05	-	-	-	69.07	-	-	27.39	3.15	-	100.66	$(Pd_{7.66}Cu_{0.19})_{7.85}(Sb_{2.65}As_{0.50})_{3.15}$
29		-	-	-	-	-	1.35	-	69.32	-	-	26.97	3.13	-	100.77	$(Pd_{7.73}Ag_{0.15})_{7.88}(Sb_{2.62}As_{0.50})_{3.12}$
30	Electrum	-	-	-	-	67.44	32.78	-	-	-	-	-	-	-	100.22	$Au_{0.53}Ag_{0.47}$
31		-	-	-	-	63.87	35.04	-	-	-	-	-	-	-	98.91	$Au_{0.50}Ag_{0.50}$
32		-	-	-	-	55.5	41.77	-	-	-	-	-	-	-	97.27	$Au_{0.58}Ag_{0.42}$

Note. "–"—below detection limit.

Table 4. Content of ore elements (wt%) and PGE (ppb) in mafic-ultramafic massifs of the Khangai upland.

№	Intrusion	Name of Rock	Sample	S wt%	Ni wt%	Cu wt%	Co wt%	Cr wt%	Pt ppb	Pd ppb	Ir ppb	Os ppb	Rh ppb	Ru ppb	Au ppb
Oortsog															
1	1	Ol mezogabbro	M01-16	0.340	0.007	0.005	-	0.060	2.72	7.55	0.02	0.96	0.11	2.64	0.62
2		Ol mezogabbro	M03-16	0.220	0.005	0.004	-	0.060	2.12	10.10	0.04	0.07	0.30	3.22	1.53
3		Ol melanogabbro	M05-16	0.310	0.009	0.006	-	0.070	4.36	1.78	0.07	0.61	0.05	0.92	0.99
4	2	melanogabbro	B-13043	0.250	0.040	0.010	-	0.110	13.00	8.00	0.30	1.60	0.20	1.30	0.00
5		mezogabbro	B-13052	0.430	0.040	0.012	-	0.140	12.00	12.00	0.20	0.57	0.10	0.60	0.00
6		mezogabbro	B-13060	0.180	0.040	0.007	-	0.150	8.00	14.00	0.22	0.14	0.30	0.80	0.00
Dulaan															
7		Ol mezogabbro	Ch41-14	0.210	0.004	0.006	0.005	0.007	1.37	2.12	0.09	0.21	0.04	0.06	-
8		Ol mezogabbro	Ch43-14	0.400	0.008	0.027	0.006	0.005	1.38	1.62	0.07	0.18	0.04	0.04	-
Mankhan															
9		leucogabbro	Sh138-17	0.310	0.004	0.013	0.005	0.004	1.54	1.43	0.09	0.14	0.04	< 1	-
10		mezogabbro	Sh143-17	0.520	0.004	0.015	0.005	0.002	1.92	0.94	0.06	0.15	0.03	< 1	-
Yamat															
11	1	mezogabbro	Sh228-14	0.590	0.012	0.287	0.005	0.010	0.94	2.08	0.09	0.27	0.08	0.85	-
12	2	Hbl mezogabbro	Sh104-14	0.320	0.010	0.033	0.006	0.017	1.71	1.90	0.08	0.21	0.11	0.13	-
13		Bt-Hbl mezog	Sh220-14/3	0.160	0.010	0.196	0.004	0.012	1.61	2.09	0.09	0.20	0.15	0.86	-
14	3	Bt-Hbl mezog-n	Sh235-14	< 0.1	0.005	0.005	0.003	0.006	1.19	2.62	0.05	0.24	0.03	0.10	-
Nomgon															
15		leucogabbro	Sh202-18	0.210	0.012	0.404	0.004	0.013	35.64	132.83	0.16	0.14	1.85	0.23	-
16		Sulfide-bearing zone I		0.600	0.022	0.341	0.005	-	114.00	388.00	-	-	2.40	-	-
17		Sulfide-bearing zone II		0.500	0.014	0.175	0.006	-	69.00	132.00	-	-	1.20	-	-
18		Sulfide-bearing zone III		0.700	0.022	0.276	0.004	-	142.00	300.00	-	-	2.60	-	-
19		Sulfide-bearing zone IV		0.130	0.028	0.857	0.007	-	190.00	540.00	-	-	3.20	-	-
Contents of Ore Elements Calculated on 100% Sulfide [1]															
Oortsog															
1	1	Ol mezogabbro	M01-16	39.96	0.76	0.59	-	-	0.320	0.888	0.002	0.113	0.013	0.310	0.073
2		Ol mezogabbro	M03-16	39.95	0.98	0.73	-	-	0.385	1.834	0.007	0.012	0.054	0.585	0.278
3		Ol melanogabbro	M05-16	39.96	1.17	0.76	-	-	0.562	0.229	0.009	0.078	0.007	0.119	0.127

Table 4. *Cont.*

4		melanogabbro	B-13043	40.16	6.43	1.62	-	-	2.088	1.285	0.048	0.257	0.032	0.209	-
5	2	mezogabbro	B-13052	40.08	3.73	1.07	-	-	1.118	1.118	0.019	0.053	0.009	0.056	-
6		mezogabbro	B-13060	40.34	8.96	1.50	-	-	1.793	3.138	0.049	0.031	0.067	0.179	-
							Dulaan								
7		Ol mezogabbro	Ch41-14	39.88	0.80	1.16	0.99	-	0.261	0.403	0.018	0.039	0.008	0.011	-
8		Ol mezogabbro	Ch43-14	39.66	0.78	2.68	0.56	-	0.138	0.161	0.007	0.018	0.004	0.04	-
							Mankhan								
9		leucogabbro	Sh138-17	39.79	0.55	1.63	0.60	-	0.198	0.183	0.012	0.019	0.005	0.013	-
10		mezogabbro	Sh143-17	39.84	0.29	1.18	0.41	-	0.147	0.072	0.004	0.011	0.003	0.008	-
							Yamat								
11	1	mezogabbro	Sh228-14	37.38	0.76	18.15	0.29	-	0.060	0.132	0.006	0.017	0.005	0.054	-
12	2	Hbl mezogabbro	Sh104-14	39.47	1.17	4.11	0.78	-	0.211	0.235	0.009	0.026	0.001	0.016	-
13		Bt-Hbl mezog.	Sh220-14/3	34.02	2.13	41.57	0.85	-	0.343	0.444	0.019	0.043	0.003	0.184	-
14	3	Bt-Hbl mezog-n	Sh235-14	38.19	18.72	20.24	11.46	-	5.557	10.005	0.198	0.923	0.013	0.384	-
							Nomgon								
15		leucogabbro	Sh202-18	31.28	1.83	60.10	0.60	-	5.213	19.785	0.024	0.022	0.028	0.004	-
16		Sulfide-bearing zone I		36.99	1.33	21.05	0.30	-	7.028	23.920	-	-	0.148	-	-
17		Sulfide-bearing zone II		38.11	1.05	13.32	0.44	-	5.259	10.060	-	-	0.091	-	-
18		Sulfide-bearing zone III		37.88	1.17	14.93	0.23	-	7.684	16.233	-	-	0.141	-	-
19		Sulfide-bearing zone IV		36.51	0.79	24.07	0.20	-	5.336	15.166	-	-	0.090	-	-

[1] Calculation method described in [57]. Note. The content of ore components from sulfide-bearing zones of the Nomgon massif (16-19) from [22]; "–"—below detection limit.

The high Cr contents (600–1400 ppm) which exceed the clark (70–83 ppm) according to [58,59] are observed in the Oortsog massif. Minerals containing chromium are olivine and chromian spinels which are found in the Oortsog massif. The maximum contents of Cu (4035 ppm) are found in the Nomgon massif while maximum contents of Ni (up to 400 ppm) are found in the Oortsog massif. Consequently, the highest values of Ni/Cu ratios are in the rocks of the Oortsog, and the lowest in the Nomgon massifs. This suggests that the sulfide melt of the Nomgon is the most fractionated.

The high content of Co versus Ni is characteristic of the rocks of all of the studied massifs with the exception of Oortsog. The Ni/Co ratio varies, reaching a maximum (5.02) for the most fractionated Nomgon massif, while the minimum (0.7–0.9) is found in the Dulaan and Mankhan massifs with low Ni content (0.004–0.008 wt%) (Table 5). High Co content in rocks is consistent with increased content of this element in sulfides (po, pn, ccp, and py) and PGM (sperrylite, majakite) (Tables 2 and 3).

The Cu, Ni, and PGE data of all studied mafic-ultramafic massifs in the Khangai upland are plotted on chondrite-normalized [60] diagrams (Figure 8). The trough-like (PGE + Cu + Ni) patterns of all of the massifs are similar to each other and vary in copper content. The Nomgon massif has a higher fractionation between IPGE and PPGE (Figure 8e), which is consistent with the copper specialization of this ore occurrence. The Yamat massif shows the lowest Pt and Pd content in the 100% sulfide phase, in contrast to other massifs (Figure 8f).

The characteristics of PGE are given in Table 5. The average total of PGE (ΣPGE) content in rocks from the massifs of the Khangai upland (Oortsog, Dulaan, Mankhan, Yamat, and Nomgon) are 15, 3.5, 3.3, 6, and 444 ppb, respectively, and the average ΣPGE in the disseminated sulfide ores in the Nomgon intrusion is higher than in others. These are varied and are lower than those of the world's giant mafic-ultramafic complexes, such as the Neoproterozoic Jinchuan deposit (0.26–135 ppm [16]), Kalatonge (to 489 ppb [61]), Kingash (to 2.9 ppm [62]), and Permo-Triassic Talnakh deposit (39–279 ppm [63]).

The ΣPGE in rock samples shows the moderate positive correlations of Ni and Cu with S content. Figure 9a–c indicate that most of the PGEs are present in the sulfides. The results of the recalculation to 100% sulfide show that the average ΣPGE of the massifs Oortsog, Dulaan, Mankhan, Yamat, and Nomgon are 2.31, 0.93, 0.92, 23.34, and 30.53 ppm, respectively. It is also lower than in the Jinchuan, Kalatonge, Kingash, and Talnakh deposits, but these are similar to the Cu–Ni sulfide deposits of Jinchuan and Kambalda, whereas the sulfide-bearing rocks of the Nomgon massif enriched in PPGE (Figure 8e) are similar to those of the Talnakh deposit (Figure 8f).

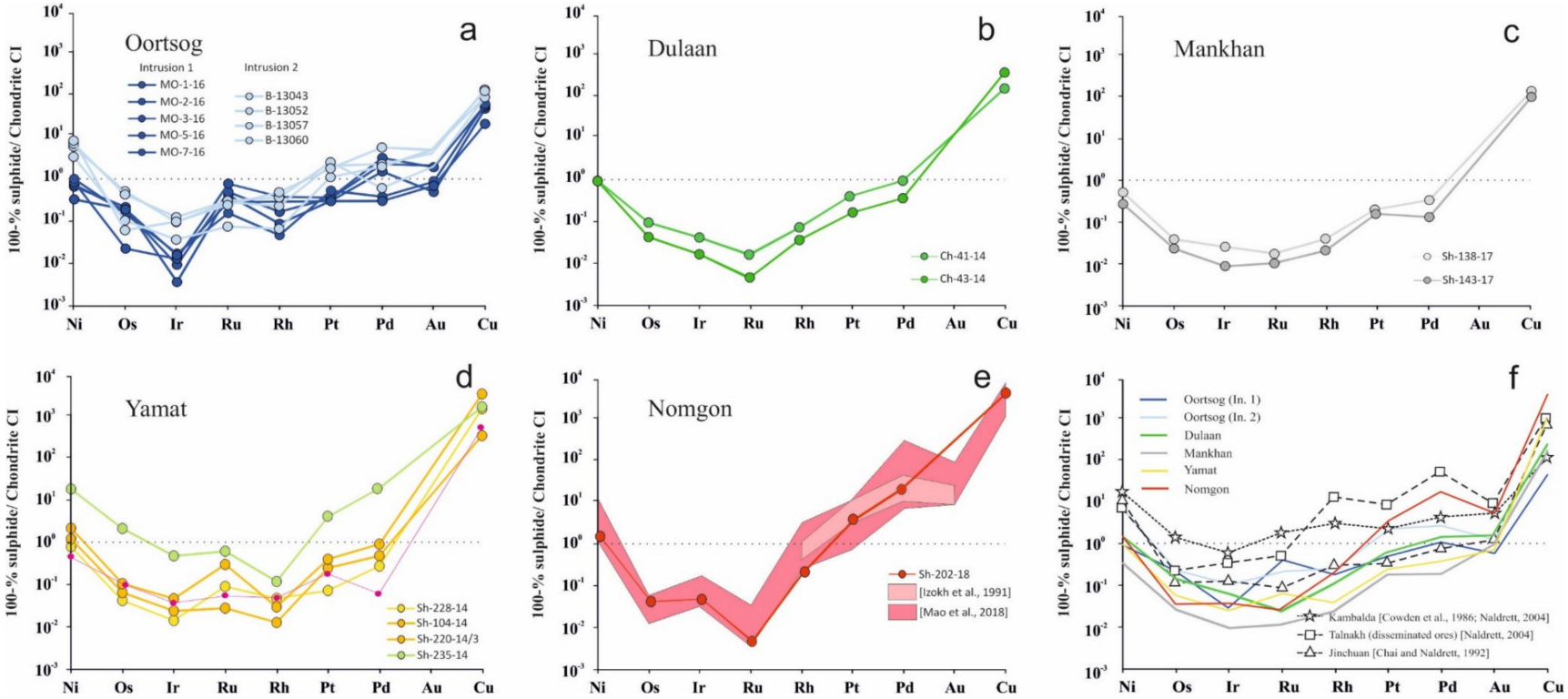

Figure 8. Chondrite normalized chalcophile-element distribution patterns for the mafic-ultramafic massifs of the Khangai upland in comparison with ores of other deposits related to ultramafic (Kambalda) and mafic (Talnakh, Jinchuan). All compositions are recalculated to 100% sulfide. References are given in Table 5. (**a**) Oortsog; (**b**) Dulaan; (**c**) Mankhan; (**d**)Yamat; (**e**) Nomgon; (**f**) massifs of the Khangai upland and other deposits.

Table 5. Characteristics of sulfide-bearing rocks of mafic-ultramafic massifs of the Khangai upland.

№	In.	Rock	Samples	∑PGE, ppb	Pt/Pd	PPGE/ IPGE	Pd/Ir	Cu/Pd (×1000)	Ni/Cu	Cu/S	Ni /Co
Oortsog											
1	1	Ol mezogabbro	MO1-16	15.42	0.36	2.84	450.79	6.62	1.30	68.00	-
2		Ol mezogabbro	MO3-16	16.82	0.21	3.68	266.10	3.96	1.35	55.00	-
3		Ol melanogabbro	MO5-16	9.07	2.45	3.83	25.15	33.15	1.54	52.54	-
4	2	melanogabbro	B13043	24.40	1.63	6.56	26.67	12.63	3.9	24.75	-
5		mezogabbro	B13052	25.47	1.00	17.52	60.00	9.58	3.48	37.39	-
6		mezogabbro	B13060	23.46	0.57	18.97	63.64	4.79	5.97	26.87	-
Dulaan											
7		Ol mezogabbro	Ch41-14	3.90	0.64	8.77	22.82	28.72	0.69	34.43	0.81
8		Ol mezogabbro	Ch43-14	3.35	0.85	8.85	22.03	166.30	0.29	14.81	1.41
Mankhan											
9		leucogabbro	Sh138-17	3.35	1.08	7.82	15.07	89.03	0.34	24.41	0.91
10		mezogabbro	Sh143-17	3.20	2.03	8.49	17.10	163.03	0.25	33.77	0.70
Yamat											
11	1	mezogabbro	Sh228-14	4.32	0.45	2.34	23.80	1375.73	0.04	2.06	2.61
12	2	Hbl mezogabbro	Sh104-14	4.05	0.89	8.36	24.75	175.01	0.29	9.61	1.51
13		Bt-Hbl mezog.	Sh220-14/3	4.87	0.77	3.17	23.99	935.35	0.05	0.82	2.50
14	3	Bt-Hbl mezog-n.	Sh235-14	8.21	0.45	9.59	50.48	20.23	0.92	1.89	1.63
Nomgon											
15		leucogabbro	Sh202-18	186.63	0.26	8.93	822.15	30.38	0.03	0.52	3.08
16		Sulfide-bearing zone I		504.40	0.29	-	-	8.80	0.06	1.76	4.48
17		Sulfide-bearing zone II		202.20	0.52	-	-	13.24	0.08	2.86	2.38
18		Sulfide-bearing zone III		444.60	0.47	-	-	9.20	0.08	2.54	5.02
19		Sulfide-bearing zone IV		733.20	0.35	-	-	15.87	0.03	1.52	4.00

Note. Characteristics for sulfide-bearing zones of the Nomgon massif (16–19) are given in [22]; "–"—below detection limit.

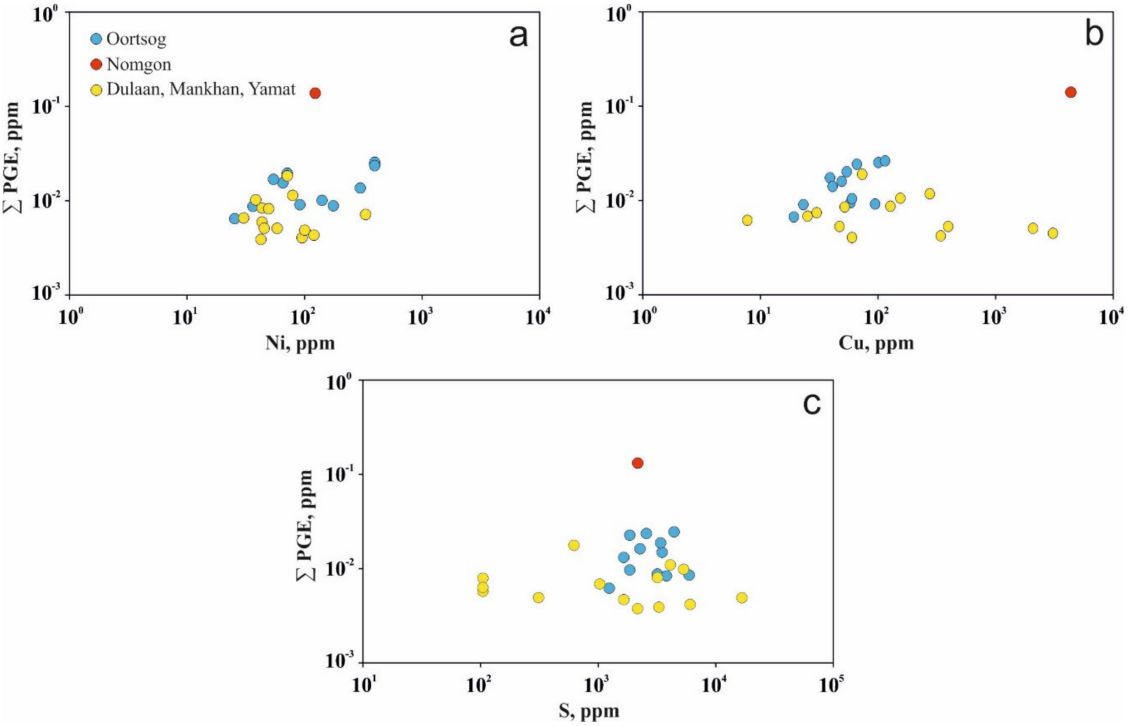

Figure 9. Correlation of ΣPGE vs. Ni (**a**), Cu (**b**), S (**c**) of the studied samples.

6. Discussion

The Permian ultramafic-mafic massifs, relating to the Khangai large igneous province, are part of the large Khangai batholith, or rather, the early phases of its formation. These massifs are the result of deep plume activity and consequently are derivatives of mantle magmatism [15–17]. Therefore, these massifs have ore (PGE-Cu-Ni) potential. Our research has indicated that all massifs refer to a common trend in the fractionation of igneous rocks, varying in composition from peridotite, troctolite, and gabbronorite to melanocratic and leucocratic gabbro [45,46]. The Oortsog massif is the most fully fractionated, while rocks of the Mankhan and Nomgon massifs refer to a more fractionated part of the general trend (Figure 3).

All massifs contain disseminated sulfide ores of various geochemical associations from chalcopyrite-pentlandite-pyrrhotite (Oortsog, Dulaan) to bornite-cubanite-chalcopyrite (Nomgon, Mankhan). A coordinated fractionation of silicate magma and sulfide melt occurs.

The Khangai magmatic province was formed by a plume [30,64] with its characteristic metallogeny. We assume that the studied PGE-Cu-Ni massifs localized in a common structure of the CAOB are products of Permian magmatism relating to the large igneous province (Khangai LIP) and to a new magmatic mafic-ultramafic formation.

6.1. Sulfides

During the process of fractionation of igneous rocks and the evolution of sulfide melt in the massifs of the Khangai upland, the composition of pyrrhotite changes from troilite to hexagonal pyrrhotite (FeS => Fe_9S_{10}). Exsolution of hexagonal pyrrhotite with enclosed troilite lamellas is a low-temperature process (from ~300 to 100 °C and lower), due to the subsolidus transformations of the initial high-temperature monosulfide solid solution (MSS) [65]. Such exsolutions were found in the ores of Cu-Ni-PGE occurrences, such as Kingash in Siberia [66], the Suoi Cun intrusion in Northeastern Vietnam [67]. The Fe content in pentlandite decreases with increasing Ni content (Figure 10) during the change of assemblages in the troilite–hexagonal pyrrhotite series. In general, the Fe/Ni ratios in the pentlandite from the Oortsog and Yamat massifs vary within ranges of

0.97–1.44 and 0.98–1.79, respectively. Pentlandite from Cu-Ni-PGE deposits is characterized by similar compositions (increased Fe content): Kingash, Yoko-Dovyren, and other massifs of the southern border of the Siberian Craton [4,7].

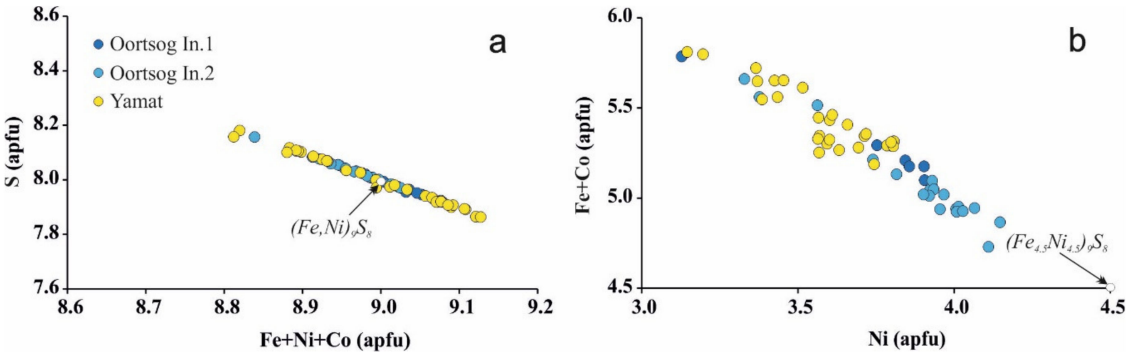

Figure 10. Chemical compositions of pentlandites in rocks of the Oortsog and Yamat massifs: a Fe+Ni+Co vs. S; b Ni vs. Fe + Co. apfu—atoms per formula unit.

The Ni/(Ni + Fe) ratio in pentlandite increases during the evolution of sulfide melt in the massifs of the Khangai upland. It was shown that in pentlandite from the Oortsog massif this ratio varies from 0.38 (in Ol-melanogabbro) to 0.52 (in leucogabbro), indicating its evolution in the range of sulfur fugacity ($lgfS_2$) from −12 to −9 at an initial temperature of pentlandite crystallization of about 600 °C [68] and its gradual decrease to 300 °C [69]. A typomorphic feature of the ore assemblage of the studied massifs is the high content Co in pentlandite, up to 15 wt%. In some analyses of pentlandite from the Oortsog massif, the Co content exceeds the sum of (Fe + Ni) and up to 45.99 wt%. Such pentlandite has been described as cobaltpentlandite [50]. The Co/Ni ratio in pentlandite increases from melanocratic to leucocratic rocks, that is, the increase of the Ni/Fe ratio indicates the increase of ($lgfS_2$) during the evolution of the ore-forming system from 600 to 200 °C [70].

Sulfide mineralization (Figure 5) in the massifs of the Khangai upland was formed according to the evolution of Fe-Ni-Cu-S system [53,71–73]. Monosulfide solid solutions (MSS) exsolved to form pyrrhotite and pentlandite [72,74] with minor chalcopyrite that is characteristic of Oortsog and Yamat (Intrusion 1) massifs. Troilite is changed by hexagonal Ni-bearing pyrrhotite, and the amount of chalcopyrite in phenocrysts increases during the differentiation of rocks from peridotites to leucogabbro, i.e., Tr + Pn(Fe > Ni) ± Ccp ≥ Po + Pn(Fe(Fe < Ni) + Ccp. Evolution of the intermediate solid solutions (iss) occurs in Mankhan, Dulaan, and Yamat (late intrusions) massifs. ISS exsolved to form a large grains of chalcopyrite with cubanite lamellae (Figure 5h) and pyrrhotite (±cbn, ±pn, ±pyrite) [57]. Cubanite results as an exsolution from chalcopyrite at temperatures below 200–210 °C [75]. The association of Cbn-Bn-Ccp with residual rare inclusions of pyrrhotite and single grains of pentlandite becomes stable when the temperature decreases similar to that observed in the Nomgon massif (Figure 5i). Such bornite containing the lamellar chalcopyrite inclusions (Figure 5i) as solid-state exsolution of iss [76,77]. This bornite is different from the secondary one [77,78]. Thus, the formation of sulfide mineralization with various assemblages took place in the process of crystallization differentiation of massif rocks. The assemblages change with an increase in the proportion of the chalcopyrite component and with a change of the composition of sulfide: an increase S in pyrrhotite and Ni in pentlandite. This trend is due to the increase of sulfur fugacity ($lgfS_2$) and the enrichment of sulfide melts with copper during the development of the ore-forming system [69,79–81]. Therefore, mineral associations change in the massifs depending on the degree of fractionation of sulfide-magmatic melts that are sequentially supplied from the intermediate chamber.

6.2. PGE Minerals

The typomorphic characteristic of PGMs for the Nomgon massif is Rh- and Os-bearing sperrylite (Table 3, [82]), similar to sperrylite from the East Siberian metallogenic province (massifs Kingash, Ognitsky, and Tartaysky) [4,6]. This sperrylite also contains refractory elements (Ir and Os), which indicates the high degree of melting of the mantle substrate. In addition to rhodium, sperrylite is gradually enriched with As, up to hollingworthite formation [83]. Grains of the hollingworthite [(Rh > Pt > Os)AsS] with Pt (up to 31 wt%) and Os (2.4 wt%) were qualitatively identified by EDS spectrometry. As a result of S-for-As substitution, sulfarsenide and sperrylite define a continuous solid-solution series from $PtAs_2$ to RhAsS in the system S-PGE-As. It is most likely that platinum enters hollingworthite in the form of a sperrylite rather than a hollingworthite minal, which is confirmed by an excess of arsenic in sulfoarsenides containing Pt. Sperrylite, in turn, contains S (0.6–2.1 wt%), but natural Pt-bearing hollingworthite and sperrylite phases show only limited solid solution (Figure 11) in which a miscibility gap exists, such as between sulfide and arsenide melts [84–89]. These partial solid solutions between arsenides and sulfarsenides were earlier reported as intermediate $PtAs_2$-PtAsS and OsS_2-OsAsS solid solutions from the Koryak-Kamchatka platinum belt [90], and between sulfides and sulfarsenides as intermediate RuS_2-IrAsS compositions in places in the northwestern Salair Ridge in Russia [91].

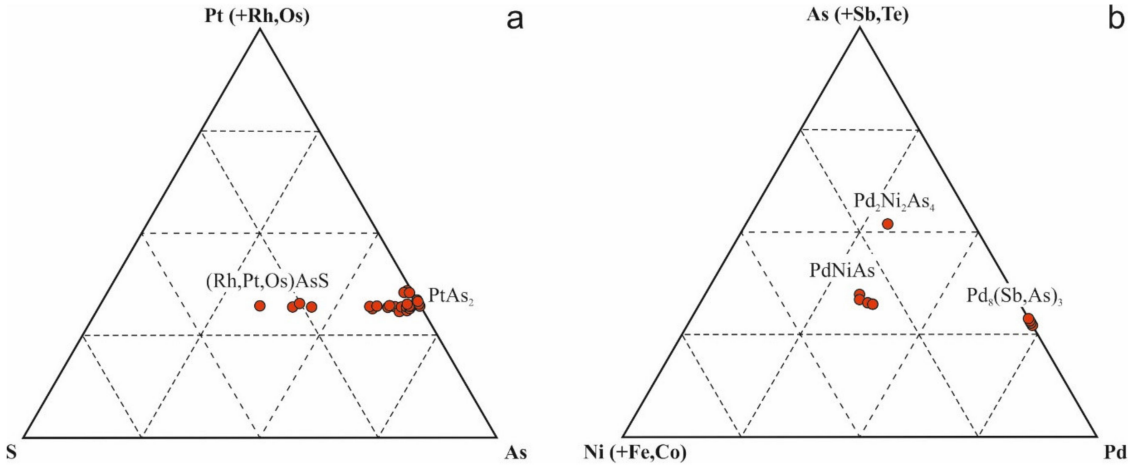

Figure 11. Composition of PGE minerals in the Nomgon massif: (**a**) solid solution of sperrylite $PtAs_2$-hollingworthite (Rh,Pt,Os)AsS; (**b**) PGE mineral paragenesises for the Ni-As-Pd system.

Pt associates with As^{n-} in preference to S^{2-} well before arsenide saturation is reached because Pt is poorly soluble when As is added to the system [92]. Unlike the other metalloid ligands, As may be present as a cation and an anion. Thus, arsenide of metals can form RhAsS when a sulfur deficit is in the bulk system [93].

Minerals of Pt predominate over Pd minerals in the disseminated chalcopyrite-pentlandite-pyrrhotite assemblage of the Oortsog massif, such as isoferroplatinum and sperrylite, and Ni-bearing sulfide of PGE (braggite) present among minerals. In contrast, the Pt minerals are in a subordinate amount compared with Pd minerals (Figure 11b) (mertieite-II, froodite, majakite, etc., in the cubanite-bornite-chalcopyrite assemblage of the Nomgon massif [23]) (Table 3). The assemblage of minerals from the Nomgon massif is comparable to the chalcopyrite ores of the Southern 2 orebody of the Talnakh intrusion [55,63]. This regularity can be explained by a direct correlation ratio of Cu/Ni vs. Pd/Pt during fractionation of sulfide melt [16,53].

6.3. Ore Geochemisrtry

The ratios of PPGE/IPGE or (Pt + Pd)/(Ru + Ir + Os) (K) and Ni/Cu ratios in ores are determined by the degree of fractionation of the sulfide melt. Ultramafic intrusions are characterized, as a rule, by low

K values and Ni/Cu ratios > 7: in Kambalda ores (Western Australia) K = 2.1, and Ni/Cu = 13.8 [16,94]; and in Thompson ores (Canada) (K = 4.4, Ni/Cu = 21.6 [16]. In contrast, mafic intrusions have higher K values and Ni/Cu ratios < 2: K = 59, Ni/Cu = 0.7 in disseminated ores of taxitic gabbro-dolerite from the Talnakh deposit (Russia) [16]; and in Jinchuan (China) K = 7.7–14.8, Ni/Cu = 1.4 [95].

Our data (Table 5) show that sulfide mineralization of the Oortsog massif was formed from a weakly fractionated melt (K = 2.84–3.87 in Intrusion 1 and K = 6.56–18.97 in Intrusion 2) compared to the Nomgon massif, in which the degree of fractionation is much higher (K = 8.93–69.30 [18]) and corresponds to the referenced mafic intrusions. The rocks of the Oortsog massif (Intrusion 1) are comparable to the Kambalda deposit in terms of the K index, and the rocks of Intrusion 2 are close to the characteristics of ores in the Jinchuan deposit, Western China.

In terms of Ni/Cu ratios (1.30–3.96), the ores of the Oortsog massif are also comparable with the characteristics of the Jinchuan deposit [95], in addition to other deposits in northwestern China [18,96]. In contrast, the ores of the Nomgon massif in terms of Ni/Cu ratios (0.03–0.08) and K are close to disseminated ores from taxite gabbro-dolerites of the Norilsk-1 intrusion [16,55]. The rocks of the other massifs (Dulaan, Mankhan, and Yamat) in Ni/Cu ratios (0.04–0.9) are close to Talnakh and PPGE/IPGE ratio (K = 2.34–9.59) are close to Jinchuan.

The average values of all of the chondrite-normalized Cu, Ni, and PGE for the massifs of the Khangai upland are plotted in Figure 8f and compared with the world's deposits. Patterns of the Oortsog, Dulaan, Mankhan, and Yamat are similar to Cu–Ni sulfide deposits (Jinchuan and Kambalda [16]) and also to other ore-enriched intrusions of Northwestern China [96]. The patterns of Nomgon and later intrusions of the Yamat are similar to Talnakh deposits [16].

The Nomgon massif has greater potential for the formation of PGE-bearing ores due to the high degree of fractionation of the sulfide melt because PGE accumulates in the residual Co-rich melts [97]. This is consistent with the fact that the PGE content (particularly Pt and Pd) in the Nomgon massif predominates over its content in other massifs (Tables 4 and 5). That is confirmed by numerous finds of PGM (Table 3) [22,23]. The Oortsog massif can also be considered as prospective for the presence of PGE, since the accumulations of PGE-enriched sulfides in the slightly eroded parts of the massif have been observed. The finds of PGMs in bedrock and in stream concentrate confirm this (Figure 7).

6.4. Parental Magmas

Ir, Ru, Os, and Ni are more compatible than Rh, Pt, Pd, and Cu during partial melting of the mantle [57,98]. Thus, magma formed by a high degree of partial melting of the mantle would result in relatively high Ni/Cu and low Pd/Ir ratios. Most sulfide-mineralized samples from the Khangai upland have moderate Ni/Cu ratios (1.30–5.97 for Oortsog, 0.03–0.92 for other massifs) and Pd/Ir ratios of 15 to 822. Most of the samples from the Khangai upland are plotted (Figure 12) within the field of high-Mg basalts, with the exception of those where Cu content is high (Nomgon and several samples of the Yamat massif (Table 5), indicating that the primary magmas of the intrusion were likely high-Mg basaltic in composition.

The sulfide ores of the Oortsog massifs (in 100% sulfide) have high Ni (0.7–8.9 wt%) and PGE contents (480–4970 ppb) the same as the most significant PGE–Ni–Cu deposits (Figure 8f), and thus high Ni/Cu ratios that indicate the enrichment of parental magmas with nickel and PGE. The Ni content and Ni/Cu ratio will decrease during fractional crystallization of olivine and pyroxenes from a basaltic magma because Ni is compatible, whereas Cu is relatively incompatible in this process [57,99]. Therefore, we propose that the primary magma of the Oortsog massif was sourced from a Ni-rich magma with a high degree of mantle partial melting. However, other massifs have much lower Ni/Cu ratios (from 0.92 to 0.03) due to high Cu (1.2–60.1 wt%). The primary magma of other massifs (Dulaan, Mankhan, Yamat, and Nomgon) was sourced from a Cu-rich magma resulting from consistent fractionation of primary magma [57].

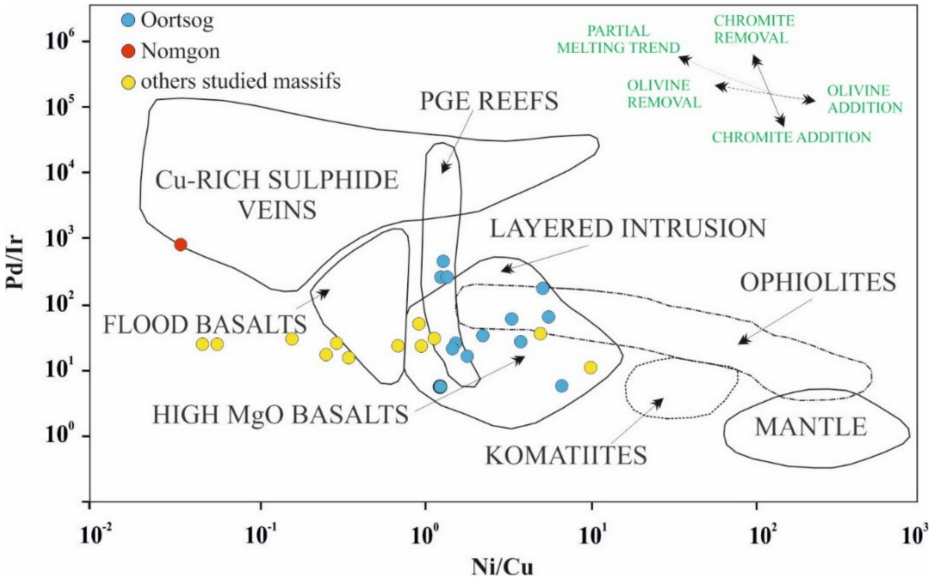

Figure 12. Plot of Pd/Ir vs. Ni/Cu for rocks from massifs of the Khangai upland. The fields are taken from [57].

7. Conclusions

(1) The Permian ultramafic-mafic massifs bearing the PGE-Cu-Ni mineralizations Oortsog, Dulaan, Mankhan, Yamat, and Nomgon relate to the Khangai large igneous province as early phases of formation of the Khangai batholith. For the first time we consider these massifs as a single magmatic association. The compositions of their rocks have a common trend in fractionation from peridotite to gabbro. They have similar typomorphic ore mineralogical and geochemical features, which differ depending on the degree of fractionation of rocks and, as a consequence, the degree of evolution of the sulfide melt.

(2) The least fractionated Oortsog massif formed from Ni-rich high-Mg basaltic magma is characterized by predominantly pyrrhotite mineralization as a result of the evolution of the MSS. The most fractionated is the Nomgon massif formed from Cu-rich basaltic magma with bornite-chalcopyrite mineralization formed as a result of the exsolution of ISS. Other massifs have a medium characteristic between these two massifs.

(3) The compositions of sulfides in the studied massifs change in accordance with the increase in sulfur fugacity from peridotite to gabbro in massifs: enrichment of pentlandite in nickel and pyrrhotite in sulfur. In the same direction, the composition of PGMs changes from Pt minerals (Oortsog massif) to Pd minerals (Nomgon massif).

(4) Mafic-ultramafic massifs related to the Khangai LIP can be considered as potential for the PGE.

Author Contributions: M.S. conceived and designed the study, interpreted the results, and wrote this article; N.T. provided valuable ideas for the discussion and edited the manuscript; R.S. provided the field work on the massifs of Khangai upland; V.K. and R.S. provided and prepared some samples for research. All authors have read and agreed to the published version of the manuscript.

Funding: The studies were carried out within the framework of the state assignment of the V.S. Sobolev Institute of Geology and Mineralogy of Siberian Branch of Russian Academy of Sciences financed by Ministry of Science and Higher Education of the Russian Federation. The reported study was funded by RFBR, project number 19-35-90033.

Acknowledgments: We are grateful to A. Izokh, M. Podlipsky, and Ya. Shelepov for their help in the field trip, samples' preparation and valuable advices. The authors thank N. Karmanova, O. Khmel'nikova, M. Khlestov, A. Titov, G. Pogudina, T. Voronova, O. Proydakova, V. Vlasova, and Yu. Sokol'nikova for received analyses.

Conflicts of Interest: The authors declare no conflict of interest.

References

1. Abbott, D.H.; Isley, A.E. The intensity, occurrence, and duration of superplume events and eras over geological time. *J. Geodyn.* **2002**, *34*, 265–307. [CrossRef]
2. Maier, W.D. Platinum-group element (PGE) deposits and occurrences: Mineralization styles, genetic concepts, and exploration criteria. *J. Afr. Earth Sci.* **2005**, *41*, 165–191. [CrossRef]
3. Dobretsov, N.L.; Borisenko, A.S.; Izokh, A.E.; Zhmodik, S.M. A thermochemical model of Eurasian Permo-Triassic mantle plumes as a basis for prediction and exploration for Cu-Ni-PGE and rare-metal ore deposits. *Russ. Geol. Geophys.* **2010**, *51*, 903–924. [CrossRef]
4. Polyakov, G.V.; Tolstykh, N.D.; Mekhonoshin, A.S.; Izokh, A.E.; Podlipskii, M.Y.; Orsoev, D.A.; Kolotilina, T.B. Ultramafic-mafic igneous complexes of the Precambrian East Siberian metallogenic province (southern framing of the Siberian craton): Age, composition, origin, and ore potential. *Russ. Geol. Geophys.* **2013**, *54*, 1319–1331. [CrossRef]
5. Ernst, R.E.; Jowitt, S.M. Large Igneous Provinces (LIPs) and metallogeny. *Soc. Econ. Geol. Spec. Publ.* **2013**, *17*, 17–51.
6. Mekhonoshin, A.S.; Tolstykh, N.D.; Podlipsky, M.Y.; Kolotilina, T.B.; Vishnevsky, A.V.; Benedyuk, Y.P. PGE mineralization of dunite-wehrlite massifs at the Gutara-Uda interfluve, Eastern Sayan. *Geol. Ore Depos.* **2013**, *55*, 162–175. [CrossRef]
7. Tolstykh, N. PGE mineralization in marginal sulfide ores of the Chineisky layered intrusion, Russia. *Mineral. Petrol.* **2008**, *92*, 283–306. [CrossRef]
8. Borisenko, A.S.; Sotnikov, V.I.; Izokh, A.E.; Polyakov, G.V.; Obolensky, A.A. Permo-Triassic mineralization in Asia and its relation to plume magmatism. *Russ. Geol. Geophys.* **2006**, *47*, 170–186.
9. Izokh, A.E.; Polyakov, G.V.; Hoa, T.T.; Balykin, P.A.; Phuong, N.T. Permian-triassic ultramafic-mafic magmatism of Northern Vietnam and Southern China as expression of plume magmatism. *Russ. Geol. Geophys.* **2005**, *46*, 922–932.
10. Shellnutt, J.G. The Emeishan large igneous province: A synthesis. *Geosci. Front.* **2014**, *5*, 369–394. [CrossRef]
11. Yarmolyuk, V.V.; Kozlovsky, A.M.; Savatenkov, V.M.; Kovach, V.P.; Kozakov, I.K.; Kotov, A.B.; Lebedev, V.I.; Eenjin, G. Composition, sources, and geodynamic nature of giant batholiths in Central Asia: Evidence from the geochemistry and Nd isotopic characteristics of granitoids in the Khangai zonal magmatic area. *Petrology* **2016**, *24*, 433–461. [CrossRef]
12. Izokh, A.E.; Vishnevskii, A.V.; Polyakov, G.V.; Shelepaev, R.A. Age of picrite and picrodolerite magmatism in western Mongolia. *Russ. Geol. Geophys.* **2011**, *52*, 7–23. [CrossRef]
13. Shelepaev, R.A.; Polyakov, G.V.; Izokh, A.E.; Vishnevsky, A.V.; Egorova, V.V.; Shelepov, Y.Y. *The Perm Intraplate Mafic-Ultramafic Associations of Asia. Materials of Conference. Correlation of Altaides and Uralides: Magmatism, Metamorphism, Stratigraphy, Geochronology, Geodynamics and Metallogeny*; Publishing House SB RAS: Novosibirsk, Russia, 2016; pp. 214–216. (In Russian)
14. Yarmolyuk, V.V.; Kuzmin, M.I.; Ernst, R.E. Intraplate geodynamics and magmatism in the evolution of the Central Asian Orogenic Belt. Journal of Asian Earth Sciences. *J. Asian Earth Sci.* **2014**, *93*, 158–179. [CrossRef]
15. Pirajno, F. *Ore Deposits and Mantle Plumes*; Kluwer Academic: Dordrecht, the Netherlands; Boston, MA, USA, 2000; p. 556.
16. Naldrett, A.J. *Magmatic Sulfide Deposits: Geology, Geochemistry and Exploration*; Springer: New York, NY, USA, 2004; p. 730.
17. Begg, G.C.; Hronsky, J.A.M.; Arndt, N.T.; Griffin, W.L.; O'Reilly, S.Y.; Hayward, N. Lithospheric, Cratonic, and Geodynamic Setting of Ni-Cu-PGE Sulfide Deposits. *Econ. Geol.* **2010**, *105*, 1057–1070. [CrossRef]
18. Mao, Y.J.; Dash, B.; Qin, K.Z.; Bujinlkham, B.; Tang, D.M. Comparisons among the Oortsog, Dulaan, and Nomgon mafic-ultramafic intrusions in central Mongolia and Ni-Cu deposits in NW China: Implications for economic Ni-Cu-PGE ore exploration in central Mongolia. *Russ. Geol. Geophys.* **2018**, *59*, 1–18. [CrossRef]
19. Tolstykh, N.D.; Podlipsky, M.Y. Heavy concentrate halos as prospecting guides for PGE mineralization. *Geol. Ore Depos.* **2010**, *52*, 196–214. [CrossRef]
20. Sal'nikova, E.B.; Yakovleva, S.Z.; Kotov, A.B.; Tolmacheva, E.V.; Plotkina, Y.V.; Fedoseenko, A.M.; Kozlovskii, A.M.; Yarmolyuk, V.V. Crystallogenesis of zircon in alkaline granites and specifics of zircon U-Pb dating: A case study of the Khangai magmatic area. *Petrology* **2014**, *22*, 450–461. [CrossRef]

21. Izokh, A.E.; Polyakov, G.V.; Krivenko, A.P.; Bognibov, V.I.; Bayarbileg, L. *The Gabbro Formation of Western Mongolia*; Nauka: Novosibirsk, Russia, 1990; p. 269. (In Russian)
22. Izokh, A.E.; Polyakov, G.V.; Anoshin, G.N.; Golovanova, N.P. Geochemistry Of Platinum Group-Metals, Gold And Silver In Nomgonsky Troctolite-Anorthozite-Gabbro Massif (Mongolia). *Geochemistry* **1991**, *10*, 1398–1405.
23. Izokh, A.E.; Mayorova, O.N.; Lavrentiev, Y.G. Minerals of the platinum metals in the Nomgon troctolite–anorthozite–gabbro intrusive massif (Mongolia). *Russ. Geol. Geophys.* **1992**, *33*, 104–110.
24. Sengor, A.M.C.; Natalin, B.A.; Burtman, V.S. Evolution of the Altaid Tectonic Collage and Paleozoic Crustal Growth in Eurasia. *Nature* **1993**, *364*, 299–307. [CrossRef]
25. Sengor, A.M.C.; Natal'in, B.A. Palaeotectonics of Asia: Fragments of a synthesis. In *Tectonic Evolution of Asia*; Yin, A., Harrison, M., Eds.; Cambridge University Press: Cambridge, UK, 1996; pp. 486–640.
26. Xiao, W.J.; Zhang, L.C.; Qin, K.Z.; Sun, S.; Li, J.L. Paleozoic accretionary and collisional tectonics of the Eastern Tianshan (China): Implications for the continental growth of Central Asia. *Am. J. Sci.* **2004**, *304*, 370–395. [CrossRef]
27. Windley, B.F.; Alexeiev, D.; Xiao, W.J.; Kroner, A.; Badarch, G. Tectonic models for accretion of the Central Asian Orogenic Belt. *J. Geol. Soc.* **2007**, *164*, 31–47. [CrossRef]
28. Kruk, N.N.; Rudnev, S.N.; Vladimirov, A.G.; Shokalsky, S.P.; Kovach, V.P.; Serov, P.A.; Volkova, N.I. Early-Middle Paleozoic granitoids in Gorny Altai, Russia: Implications for continental crust history and magma sources. *J. Asian Earth Sci.* **2011**, *42*, 928–948. [CrossRef]
29. Safonova, I.; Seltmann, R.; Kroner, A.; Gladkochub, D.; Schulmann, K.; Xiao, W.J.; Kim, J.; Komiya, T.; Sun, M. A new concept of continental construction in the Central Asian Orogenic Belt (compared to actualistic examples from the Western Pacific). *Episodes* **2011**, *34*, 186–196. [CrossRef]
30. Kuzmin, M.I.; Yarmolyuk, V.V. Mantle plumes of Central Asia (Northeast Asia) and their role in forming endogenous deposits. *Russ. Geol. Geophys.* **2014**, *55*, 120–143. [CrossRef]
31. Koval, P.V.; Antipin, V.S.; Tsypukov, Y.P.; Smirnov, V.N. Geological structure and material composition of the Baga-Khenteiskiy batholith (MPR). *Russ. Geol. Geophys.* **1978**, *5*, 68–78. (In Russian)
32. Litvinovsky, B.A.; Zanvilevich, A.N.; Alakshin, A.M.; Podladchikov, Y.Y. *Angara-Vitim Batholith is the Largest Granitoid Pluton*; Science: Novosibirsk, Russia, 1992; p. 141. (In Russian)
33. Yarmolyuk, V.V.; Kovalenko, V.I.; Kozakov, I.K.; Sal'nikova, E.B.; Bibikova, E.V.; Kovach, V.P.; Kozlovsky, A.M.; Kotov, A.B.; Lebedev, V.I.; Eenjin, G.; et al. The age of the Khangai batholith and the problem of batholith formation in Central Asia. *Dokl. Earth Sci.* **2008**, *423*, 1223–1228. [CrossRef]
34. Donskaya, T.V.; Gladkochub, D.P.; Mazukabzov, A.M.; Ivanov, A.V. Late Paleozoic-Mesozoic subduction-related magmatism at the southern margin of the Siberian continent and the 150 million-year history of the Mongol-Okhotsk Ocean. *J. Asian Earth Sci.* **2013**, *62*, 79–97. [CrossRef]
35. Kovalenko, V.I.; Yarmolyuk, V.V.; Kovach, V.P.; Kotov, A.B.; Kozakov, I.K.; Salnikova, E.B.; Larin, A.M. Isotope provinces, mechanisms of generation and sources of the continental crust in the Central Asian Mobile Belt: Geological and isotopic evidence. *J. Asian Earth Sci.* **2004**, *23*, 605–627. [CrossRef]
36. Yarmolyuk, V.V.; Kozlovsky, A.M.; Sal'nikova, E.B.; Kozakov, I.K.; Kotov, A.B.; Lebedev, V.I.; Eenjin, G. Age of the Khangai batholith and challenge of polychronic batholith formation in Central Asia. *Dokl. Earth Sci.* **2013**, *452*, 1001–1007. [CrossRef]
37. Tomurtogoo, O.; Windley, B.F.; Kroner, A.; Badarch, G.; Liu, D.Y. Zircon age and occurrence of the Adaatsag ophiolite and Muron shear zone, central Mongolia: Constraints on the evolution of the Mongol-Okhotsk ocean, suture and orogen. *J. Geol. Soc.* **2005**, *162*, 125–134. [CrossRef]
38. Li, S.; Wang, T.; Wilde, S.A.; Tong, Y. Evolution, source and tectonic significance of Early Mesozoic granitoid magmatism in the Central Asian Orogenic Belt (central segment). *Earth-Sci. Rev.* **2013**, *126*, 206–234. [CrossRef]
39. Ernst, R.E. *Large Igneous Provinces*; Cambridge University Press: Cambridge, UK, 2014; pp. 1–653.
40. Tang, G.J.; Chung, S.L.; Hawkesworth, C.J.; Cawood, P.A.; Wang, Q.; Wyman, D.A.; Xu, Y.G.; Zhao, Z.H. Short episodes of crust generation during protracted accretionary processes: Evidence from Central Asian Orogenic Belt, NW China. *Earth Planet. Sci. Lett.* **2017**, *464*, 142–154. [CrossRef]

41. Tsukada, K.; Nuramkhaan, M.; Purevsuren, N.; Kabashima, T.; Kondo, T.; Gantumur, O.; Hasegawa, H.; Yamamoto, K. Permian adakitic magmatism in the Khanui Group, Northern Mongolia—Late Paleozoic slab-melting of subducted oceanic plate beneath the "Siberian continent". *J. Geodyn.* **2018**, *121*, 49–63. [CrossRef]
42. Shapovalova, M.O.; Tolstykh, N.D.; Shelepaev, R.A.; Tsibizov, L.V. The Oortsog Peridotite-Troctolite-Gabbro Intrusion, Western Mongolia: New Petrological and Geochronological Constraints. *Russ. Geol. Geophys.* **2019**, *60*, 845–861. [CrossRef]
43. Shelepaev, R.A.; Egorova, V.V.; Izokh, A.E.; Vishnevsky, A.V.; Shelepov, Y.Y.; Rudnev, S.N. Permian gabbroid intrusions of the Khangai highlands (Western Mongolia). Isotope dating of geological processes: New results, approaches and prospects. In *Proceedings of the VI Russian Conference on Isotope Geochronology*; Sprinter: St. Petersburg, Russia, 2015; pp. 337–338. (In Russian)
44. Izokh, A.E.; Polyakov, G.V.; Gibsher, A.S.; Balykin, P.A.; Zhuravlev, D.Z.; Parkhomenko, V.A. High-alumina layered gabbroids of the Central-Asian fold belt: Geochemical composition, Sm-Nd isotopic age, and geodynamic conditions of formation. *Russ. Geol. Geophys.* **1998**, *39*, 1565–1577.
45. Shapovalova, M.O.; Shelepaev, R.A.; Tolstykh, N.D.; Izokh, A.E. Gabbroid massifs of the Khangai Upland as a result of the interaction of the mantle plume with the lithospheric mantle. Petrology of magmatic and metamorphic complexes. In *Proceedings of the X Russian Petrographic Conference with International Participation*; Tomsk Center for Science and Technology: Tomsk, Russia, 2018; Volume 10, pp. 428–432. (In Russian)
46. Shapovalova, M.; Shelepaev, R.; Tolstykh, N. Petrological characteristics of mafic-ultramafic intrusions of the Khangay upland (Mongolia). In Proceedings of the 15th SGA Biennial Meeting, Glasgow, Scotland, 27–30 August 2019; Volume 2, pp. 561–564.
47. Shapovalova, M.; Tolstykh, N.; Shelepaev, R.; Safonova, I. Petrologo-geochemical features of the mafic-ultramafic massifs of the Khangai upland, Western Mongolia. *J. Asia Earth Sci.* **2021**. under review.
48. Lavrent'ev, Y.G.; Karmanov, N.S.; Usova, L.V. Electron-probe determination of the composition of minerals: Microanalyzer or scanning electron microscope. *Russ. Geol. Geophys.* **2015**, *56*, 1473–1482. (In Russian) [CrossRef]
49. Lavrent'ev, Y.G.; Usova, L.V. The choice of the optimal method for calculating correction factors in X-ray microanalysis of rock-forming minerals. *J. Anal. Chem.* **1996**, *51*, 323–331. (In Russian)
50. Shapovalova, M.O.; Tolstykh, N.D.; Shelepaev, R.A. Cu-Ni-PGE mineralization of the peridotite-gabbro massif Oortsog, Western Mongolia. Ore-magmatic systems. Magmatism, metallogeny and tectonics of North Asia. Collection of scientific papers on fundamental research of the Institute of Geology and Mineralogy SB RAS. *Novosibirsk: IGM SB RAS* **2018**, *1*, 44–55. (In Russian)
51. Kuova, O.; Huhma, M.; Vuorelainen, Y. A natural cobalt analog of pentlandite. *Am. Mineral.* **1959**, *44*, 897–900.
52. Kretz, R. SYMBOLS FOR ROCK-FORMING MINERALS. *Am. Mineral.* **1983**, *68*, 277–279.
53. Likhachev, A.P. *Platinum-Copper-Nickel and Platinum Deposits*; Eslan: Moscow, Russia, 2006; p. 496. (In Russian)
54. Krivenko, A.P.; Lopukhov, A.S.; Glotov, A.I. *Geochemical Associations of Rare and Radioactive Elements in Ore and Magmatic Complexes*; Nauka: Novosibirsk, Russia, 1990; p. 55. (In Russian)
55. Tolstykh, N.; Krivolutskaya, N.; Safonova, I.; Shapovalova, M.; Zhitova, L.; Abersteiner, A. Unique Cu-rich sulphide ores of the Southern-2 orebody in the Talnakh Intrusion, Noril'sk area (Russia): Geochemistry, mineralogy and conditions of crystallization. *Ore Geol. Rev.* **2020**, *122*. [CrossRef]
56. Shapovalova, M.; Shelepaev, R.; Tolstykh, N.; Kalugin, V.; Safonova, I. Petrology of the Ortsog-Uul Gabbro-Peridotite PGE-Bearing Complex, Western Mongolia. *Min. Resour. Sustain. World* **2015**, *1–5*, 983–985.
57. Barnes, S.-J.; Lightfoot, P.C. Formation of magmatic nickel-sulphide ore deposits and processes affecting their copper and platinum-group element contents. *Econ. Geol.* **2005**, *100*, 179–213.
58. Vinogradov, A.P. The average content of chemical elements in the main types of eruptions genus of the earth's crust. *Geochemical* **1962**, *7*, 555–571. (In Russian)
59. Taylor, S.R. Abundance of chemical elements in the continental crust: A new table. *Geochim. Cosmochim. Acta* **1964**, *28*, 1273–1285. [CrossRef]
60. Anders, E.; Grevesse, N. Abundances of the elements: Meteoric and solar. *Geochim. Cosmochim. Acta* **1989**, *53*, 197–214. [CrossRef]
61. Zhang, Z.; Mao, J.; Chai, F.; Yan, S.; Chen, B.; Pirajno, F. Geochemistry of the Permian Kalatongke mafic intrusions, Northern Xinjiang, Northwest China: Implications for the genesis of magmatic Ni-Cu sulfide deposits. *Econ. Geol.* **2009**, *104*, 185–203. [CrossRef]

62. Radomskaya, T.A.; Glazunov, O.M.; Vlasova, V.N.; Suvorova, L.F. Geochemistry and mineralogy of platinum group element in ores of the Kingash deposit, Eastern Sayan, Russia. *Geol. Ore Depos.* **2017**, *59*, 354–374. [CrossRef]
63. Krivolutskaya, N.; Tolstykh, N.; Kedrovskaya, T.; Naumov, K.; Kubrakova, I.; Tyutyunnik, O.; Gongalsky, B.; Kovalchuk, E.; Magazina, L.; Bychkova, Y.; et al. World-Class PGE-Cu-Ni Talnakh Deposit: New Data on the Structure and Unique Mineralization of the South-Western Branch. *Minerals* **2018**, *8*, 124. [CrossRef]
64. Yarmolyuk, V.V.; Kuzmin, M.I.; Kozlovsky, A.M. Late paleozoic-Early Mesozoic within-plate magmatism in North Asia: Traps, rifts, giant batholiths, and the geodynamics of their origin. *Petrology* **2013**, *21*, 101–126. [CrossRef]
65. Kissin, S.A.; Scott, S.D. PHASE-RELATIONS INVOLVING PYRRHOTITE BELOW 350-DEGREES-C. *Econ. Geol.* **1982**, *77*, 1739–1754. [CrossRef]
66. Lygin, A.V. *Features of the Composition of the Ores of the Verkhnekingash Platinoid-Cobalt-Copper-Nickel Deposit (Krasnoyarsk Region)*; Moscow University: Moscow, Russia, 2010; Volume 2, pp. 69–72. (In Russian)
67. Svetlitskaya, T.V.; Tolstykh, N.D.; Izokh, A.E.; Thi, P.N. PGE geochemical constraints on the origin of the Ni-Cu-PGE sulfide mineralization in the Suoi Cun intrusion, Cao Bang province, Northeastern Vietnam. *Mineral. Petrol.* **2015**, *109*, 161–180. [CrossRef]
68. Vaughan, D.J.; Craig, J.R. *Mineral Chemistry of Sulfides*; Cambridge University Press: Cambridge, UK, 1978; p. 512.
69. Kolonin, G.R.; Orsoev, D.A.; Sinyakova, E.F.; Kislov, E.V. The use of Ni:Fe ratio in pentlandite for estimation of sulfur fugacity during the formation of PGE-bearing sulfide mineralization of Yoko-Dovyren massif. *Dokl. Akad. Nauk* **2000**, *370*, 87–91.
70. Kaneda, H.; Takenouchi, S.; Shoji, T. Stability of pentlandite in the fe-ni-co-s system. *Mineral. Depos.* **1986**, *21*, 169–180. [CrossRef]
71. Craig, J.R.; Kullerud, G. Phase relations in the Cu–Fe–Ni–S system and their application to magmatic ore deposits. *Econ. Geol.* **1969**, *4*, 344–358.
72. Kullerud, G.; Yund, R.A.; Moh, G.H. Phase relations in the Cu-Fe-S, Cu-Ni-S and Fe-Ni-S systems. In *Magmatic Ore Deposits*; Wilson, H.D.B., Ed.; Economic Geology Publishing Co.: Lancaster, PA, USA, 1969; pp. 323–343.
73. Fleet, M.E.; Pan, Y.M. Fractional crystallization of anhydrous sulfide liquid in the system Fe-Ni-Cu-S, with application to magmatic sulfide deposits. *Geochim. Cosmochim. Acta* **1994**, *58*, 3369–3377. [CrossRef]
74. Sinyakova, E.; Kosyakov, V.; Nenashev, B.; Tsirkina, N.L. Single-crystal growth of (FeyNi1-y)S1-delta solid solution. *J. Cryst. Growth* **2005**, *275*, E2055–E2060. [CrossRef]
75. Cabri, L.J. NEW DATA ON PHASE RELATIONS IN CU-FE-S SYSTEM. *Econ. Geol.* **1973**, *68*, 443–454. [CrossRef]
76. Cook, N.J.; Ciobanu, C.L.; Danyushevsky, L.V.; Gilbert, S. Minor and trace elements in bornite and associated Cu–(Fe)-sulfides: A LA-ICP-MS study Bornite mineral chemistry. *Geochim. Cosmochim. Acta* **2011**, *75*, 6473–6496. [CrossRef]
77. Ramdohr, P. *The Ore Minerals and Their Intergrowths*, 2nd ed.; International series in earth science; Pergamon Press: London, UK, 1980; Volume 35, p. 1207.
78. Robb, L. *Introduction to Ore-Forming Processes*; Blackwell Publishing: Oxford, UK, 2005; 373p.
79. Mirsa, K.; Fleet, M.E. The chemical compositions of synthetic and natural pentlandite assemblages. *Econ. Geol.* **1973**, *68*, 518–539.
80. Distler, V.V.; Genkin, A.D.; Filimonova, A.A.; Hitrov, V.G.; Laputina, I.P. The zoning of copper-nickel ores of Talnakh and Oktyabr'sky deposits. *Geol. Ore Depos.* **1975**, *2*, 16–27.
81. Makovicky, E. Ternary and quaternary phase systems with PGE. The geology, geochemistry, mineralogy and mineral beneficiation of platinum-group elements. In *CBM Special Canadian Institute of Mining, Metallurgy and Petroleum*; Cabri, L.J., Ed.; Marc Veilleux Imprimeur Inc.: Boucherville, QC, Canada, 2002; Volume 54, pp. 131–175.
82. Izokh, A.E.; Maiorova, O.N. Rhodium sperrylite from the nomgon massif (mongolia). *Dokl. Akad. Nauk* **1990**, *313*, 1212–1215.
83. Stumpel, E.F.; Clark, A.M. Hollingworthite, a new rhodium mineral, identified by electron probe microanalysis. *Am. Mineral.* **1965**, *50*, 1068–1074.
84. Lorand, J.P. Sur l'origine mantellaire de l'arsenic dans les roches du manteaux: Exemple des pyroxénites à grenat du massif lherzolitique des beni bousera (Rif, maroc). *CR Acad. Sci. Paris* **1987**, *305*, 383–386.

85. Leblanc, M.; Fischer, W. Gold and platinum group elements in cobalt-arsenide ores—Hydrothermal concentration from a serpentinite source-rock (Bou-Azzer, Morocco). *Mineral. Petrol.* **1990**, *42*, 197–209. [CrossRef]
86. Gervilla, F.; Leblanc, M.; TorresRuiz, J.; HachAli, P.F. Immiscibility between arsenide and sulfide melts: A mechanism for the concentration of noble metals. *Can. Mineral.* **1996**, *34*, 485–502.
87. Gervilla, F.; Sanchez-Anguita, A.; Acevedo, R.D.; Hach-Ali, P.F. Platinum-group element sulpharsenides and Pd bismuthotellurides in the metamorphosed Ni-Cu deposit at Las Aguilas (Province of San Luis, Argentina). *Mineral. Mag.* **1997**, *61*, 861–877. [CrossRef]
88. Gervilla, F.; Papunen, H.; Kojonen, K.; Johanson, B. Platinum-, palladium- and gold-rich arsenide ores from the Kylmakoski Ni-Cu deposit (Vammala Nickel Belt, SW Finland). *Mineral. Petrol.* **1998**, *64*, 163–185. [CrossRef]
89. Hanley, J.J. The role of arsenic-rich melts and mineral phases in the development of high-grade Pt-Pd mineralization within komatiite-associated magmatic Ni-Cu sulfide horizons at dundonald beach south, Abitibi subprovince, Ontario, Canada. *Econ. Geol.* **2007**, *102*, 305–317. [CrossRef]
90. Tolstykh, N.D.; Sidorov, E.G.; Kozlov, A.P. Platinum-group minerals in lode and placer deposits associated with the Ural-Alaskan-type Gal'moenan complex, Koryak-Kamchatka Platinum Belt, Russia. *Can. Mineral.* **2004**, *42*, 619–630. [CrossRef]
91. Tolstykh, N.D.; Lapukhov, A.S.; Krivenko, A.P.; Lazareva, E.V. Platinum-group minerals in gold placers in northwestern Salair. *Russ. Geol. Geophys.* **1999**, *40*, 916–925. (In Russian)
92. Helmy, H.M.; Ballhaus, C.; Fonseca, R.O.C.; Wirth, R.; Nagel, T.; Tredoux, M. Noble metal nanoclusters and nanoparticles precede mineral formation in magmatic sulphide melts. *Nat. Commun.* **2013**, *4*. [CrossRef]
93. Helmy, H.M.; Ballhaus, C.; Wohlgemuth-Ueberwasser, C.; Fonseca, R.O.C.; Laurenz, V. Partitioning of Se, As, Sb, Te and Bi between monosulfide solid solution and sulfide melt—Application to magmatic sulfide deposits. *Geochim. Cosmochim. Acta* **2010**, *74*, 6174–6179. [CrossRef]
94. Cowden, A.; Donaldson, M.J.; Naldrett, A.J.; Campbell, I.H. Platinum-group elements and gold in the komatiite-hosted Fe-Ni-Cu sulfide deposits at Kambalda, Western-Australia. *Econ. Geol.* **1986**, *81*, 1226–1235. [CrossRef]
95. Chai, G.; Naldrett, A.J. Characteristics of Ni-Cu-Pge Mineralization and Genesis of the Jinchuan Deposit, Northwest China. *Econ. Geol. Bullet. Soc. Econ. Geol.* **1992**, *87*, 1475–1495. [CrossRef]
96. Qin, K.-Z.; Tang, D.-M.; Su, B.-X.; Mao, Y.-J.; Xue, S.-C. The tectonic setting, stytle, basic feature, relative erosion degree, ore-bearing evaluation sign, potential analysis of mineralization of Cu-Ni bearing Permian mafic–ultramafic complexes, Northern Xinjiang. *Northwest Geol.* **2012**, *45*, 83–116.
97. Naldrett, A.J. Secular Variation of Magmatic Sulfide Deposits and Their Source Magmas. *Econ. Geol.* **2010**, *105*, 669–688. [CrossRef]
98. Barnes, S.J.; Naldrett, A.J.; Gorton, M.P. The origin of the fractionation of platinum-group elements in terrestrial magmas. *Chem. Geol.* **1985**, *53*, 303–323. [CrossRef]
99. Wei, B.; Wang, C.Y.; Li, C.; Sun, Y. Origin of PGE-depleted Ni-Cu sulfide mineralization in the Triassic Hongqiling No. 7 orthopyroxenite intrusion, Central Asian orogenic belt, northeastern China. *Econ. Geol.* **2013**, *108*, 1813–1831. [CrossRef]